# Effects of Mach Number and Flow Incidence on Aerodynamic Losses of Steam Turbine Blades

**Teik Lin Chu**

Thesis submitted to the Faculty of the
Virginia Polytechnic Institute and State University
in partial fulfillment of the requirements for the degree of

**Master of Science**
**in**
**Mechanical Engineering**

Dr. Wing Fai Ng, Chair
Dr. Clint Dancey
Dr. Doug Nelson

March 31st, 1999
Blacksburg, Virginia

Keywords: Steam Turbine, Nozzle, Aerodynamic Loss, Transonic

**Effects of Mach Number and Flow Incidence on Aerodynamic Losses of Steam Turbine Blades**

Teik Lin Chu

(ABSTRACT)

An experiment was conducted to investigate the aerodynamic losses of two high-pressure steam turbine nozzles (526A, 525B) subjected to a large range of incident angle and exit Mach number. The blades were tested in a 2D transonic windtunnel. The exit Mach number ranged from 0.60 to 1.15 and the incidence was varied from -34$^o$ to 35$^o$. Measurements included downstream Pitot probe traverses, upstream total pressure, and endwall static pressures. Flow visualization techniques such as shadowgraph photography and color oil flow visualization were performed to complement the measured data. When the exit Mach number for both nozzles increased from 0.9 to 1.1, the total pressure loss coefficient increased by a factor of 7 as compared to the total pressure losses observed at subsonic condition ($M_2$<0.9). For the range of incidence tested, the effect of flow incidence on the total pressure losses is less pronounced. Based on shadowgraphs taken during the experiment, it's believed that the large increase in losses at transonic conditions is due to strong shock/boundary layer interaction that may lead to flow separation on the blade suction surface. From the measured total pressure coefficients, a modified loss model that accounts for higher losses at transonic conditions was developed. The new model matches the data much better than the existing Kacker-Okapuu model for transonic exit conditions.

## ACKNOWLEDGEMENTS

My greatest appreciation and gratitude to my advisor Dr. Wing Fai Ng for giving me this opportunity to work on this project for my MS degree. The project is successful under his guidance and sound advice. Without those valuable assistance, this work could not have been possible.

I would also like to thank Dr. Clint Dancey and Dr. Doug Nelson for serving on my committee. The introductory class in turbomachinery and fluid mechanics conducted by Dr Dancey has given me the necessary foundation to begin my work.

Special thanks to my fellow graduate students Oliver Poop and Tom Vandepuette for assisting me with my experiments in the wind tunnel. I thank Oliver for his help with all the troubleshoot of the equipment in the wind tunnel and his valuable assistance in showing me the delicate setup of optical photography. I appreciate Tom for his help and patience in performing the tests in the wind tunnel. In addition, I would like to commend the efforts by Dr. Seok Jae Yoo and Dr. Shi Ming Lee who helped me to start this project and for their valuable advice and assistance they have given me throughout the course of my work.

Finally I would like to thank Gary Stafford for assistance in operating the electronic devices in the wind tunnel and James Dowdy for his excellent machine work.

# TABLE OF CONTENTS

## LIST OF FIGURES

## LIST OF TABLES

# NOMENCLATURE

| | |
|---|---|
| C | Chord |
| O | Throat |
| S | Pitch |
| C/S | Solidity |
| O/S | Gauging |
| $\alpha$ | Flow Angle |
| $\beta$ | Metal Angle |
| i | Incidence ($\beta_1$-$\alpha_1$) |
| PS | Pressure Side |
| SS | Suction Side |
| tmax | Maximum Blade Thickness |
| $P_o$ | Stagnation Pressure |
| Ps | Static Pressue |
| $T_o$ | Stagnation Temperature |
| Ts | Static Temperature |
| Pd | Differential Total Pressure, $P_{o1}$-$P_{o2}$ |
| M | Mach Number |
| $\rho$ | Density |
| V | Velocity |
| $\gamma$ | Specific Heat Ratio for Air |
| R | Gas Constant |
| x | Axial Distance from Trailing Edge |
| $\omega$ | Mass Averaged Total Pressure Loss Coefficient |
| $\omega_{p,ko}$ | Kacker Okapuu Loss Coefficient |
| $\omega_{shock}$ | Kacker-Okapuu Shock Loss Correlation |
| $\tau$ | Mass Averaged Kinetic Energy Loss Coefficient |
| $Y_{P,AMDC}$ | Ainley-Mathieson/Dunham-Came Loss Coefficient |

Subscripts

| | |
|---|---|
| 1 | Inlet |
| 2 | Exit |
| i | Isentropic |

# Chapter 1 INTRODUCTION

In the power generation industry gas turbines and steam turbines are widely used for generating power. These industrial machines are capable of producing power in hundreds of megawatts. The efficiency of a turbine is largely dependent on its aerodynamic performance. Hence, the design of blade profiles for nozzles and rotors are continuously improved over the decades to achieve better overall efficiency for the turbine.

Nozzles and rotors are designed to operate at a certain condition, however in actual application they are operated at off-design conditions quite frequently. This change results in the inlet flow entering the various stages in the turbine to be off incidence. Thus, profile losses generally increase which leads to the decline in overall efficiency of the turbine. Unlike a compressor, a turbine can handle a sizeable range of incidence without increasing losses significantly. This is due to the occurrence of flow acceleration in the turbine and a favorable pressure gradient. However, when operating at positive incidence, blade loading increases and this results in thicker boundary layer growth and regions of adverse pressure gradient (Venkatrayulu et al., 1989). Flow separation will occur and the profile loss increase with the loss increment depending on the extent of the flow separation.

Cascade tests have been carried out over the years to determine aerodynamic losses in turbomachines. Although the results from such tests are not as accurate as the data obtained from the tests conducted on the operating turbomachine, cascade test provides a blade designer a more economical alternative to determine the aerodynamic efficiency of the blades under various operating conditions. In addition, the cascade results are used to validate flow computation programs and to further refine their accuracy in predicting flow phenomenon in turbomachines. These programs are able to predict losses reasonably well for subsonic flow. However in transonic flow, shock-boundary layer interaction is evident and the structure of this interaction is complex and difficult to predict. Until significant progress is achieved in refining the available flow computation programs in the industry, cascade test is still an effective method to determine aerodynamic losses of turbomachines.

Experiments are carried out on VPI's transonic test-section to investigate the aerodynamic losses of the two sets of steam turbine nozzles operating at design and off-design incidence in transonic flow. Incident angles are varied from $-35^{o}$ to $+34^{o}$ for the cascade tests. The test at such a large range of incident angles is uncommon in linear cascade tests performed by most researchers. Hence, published test data at such extreme incident angles are not made available in turbomachinery journals. The exit Mach number is varied from 0.6 to 1.15. Pressure measurements such as total pressure and wall static pressure are used to compute the loss coefficient. The loss coefficient is then compared at various incidences at a specific exit Mach number. In addition, losses from the two sets of nozzles are compared based on incidence and exit Mach number. Results from turbine blades of similar profile are compared with data from the in-house steam turbine nozzles. A loss prediction method by Kacker and Okapuu is used to calculate the profile loss of the nozzles based on blade geometry and flow incidence. In addition, a proposed shock model is developed based on current experimental data to better account for the shock losses.

# Chapter 2 BACKGROUND

## 2.1 Overview

Steam turbine cascade tests are usually conducted without the compliment of steam, instead air is being used as the test medium.  VPI current setup for cascade test involves 2 types of nozzle guide vanes used in the high-pressure stage of a Rateau steam turbine.  These nozzles have a 2-D cross-section without twist and are used in multiple stages keeping similar blade profiles.  The purpose of the nozzles is to accelerate and guide the flow into the next stage of rotors.  Since a steam turbine can spend a considerable amount of time operating at off-design conditions, the mass flow in the turbine and the rotors' speed varies.  Hence, the flow entering each stage of nozzles and rotors is inclined at an incident angle.

## 2.2 Flow Field in Axial Turbines

The flow field in an axial turbine is quite complex.  Flow entering the first stage guide vanes are mainly laminar and is two-dimensional across most of the span.  At the end walls the flow is three-dimensional resulting in a horseshoe vortex formed by the interaction between the blade and endwall boundary layers.  With the flow between blade passages accelerating, the boundary layer turns transitional on the suction side of the blades.  Unlike an axial compressor, favorable pressure gradient exists between blade passages in an axial turbine due to flow acceleration.  This reduces the tendency of flow separation to occur. At the exit of each blade stage, the flow is turbulent due to wake mixing and secondary flow (Lakshminarayana, 1996).  According to Lakshminarayana (1996), free stream turbulence will likely cause the formation of transitional flow near the leading edge of blades.  Hence, leading edge blade profile can be altered to delay transition and eliminate separation bubbles.

### 2.2.1 Nature of Boundary Layers

Boundary layers in turbines are typically thin and the layer gets thinner with the increase in Reynold's number of the flow. Since the boundary layer at the inlet stage of a turbine is laminar, the friction loss from viscous interaction with the blade surface is low. However, it is more likely for a laminar boundary layer to separate when it encounters a region of adverse pressure gradient. A turbulent boundary layer will have higher viscous loss compared to a laminar one but has fewer tendencies to separate.

Blade loading is a factor that can cause a region of adverse pressure gradient to exist at the trailing edge of turbine blades on the suction surface. The adverse pressure gradient may cause the boundary layer to separate. Once the boundary layer separated there exist a region of back flow. Depending on the location and nature of the flow separation, the separated flow may re-attach itself onto the blade surface. This enclosed region is a separation bubble and on top of the bubble lies the separated shear layer as shown in Figure 2.1. After re-attachment the flow becomes fully turbulent and the boundary layer will separate near the trailing edge when incident shocks strike the suction surface.

### 2.2.2 Shock Structure and its Interaction with Boundary Layer

Shock is a form of physical discontinuity and has the appearance as thin viscous layers. It is formed at the trailing edges when the throat opening is choked (Mach number is unity). Stagnation enthalpy is unchanged across the shock whereas static enthalpy, pressure, temperature will increase across this discontinuity. Usually a fishtail shock will be evident near the trailing edge when the exit flow's Mach number exceeds unity. This shock will progress from a weak shock such as a Mach wave to stronger normal shock. Subsequently the normal shock transforms into an oblique shock when the Mach number is further increased. The shock formed on pressure surface will impinge onto the suction surface of the blade below and is reflected back as a shock. The incident shock on the suction side boundary layer will produce pressure rise and encouraging boundary layer

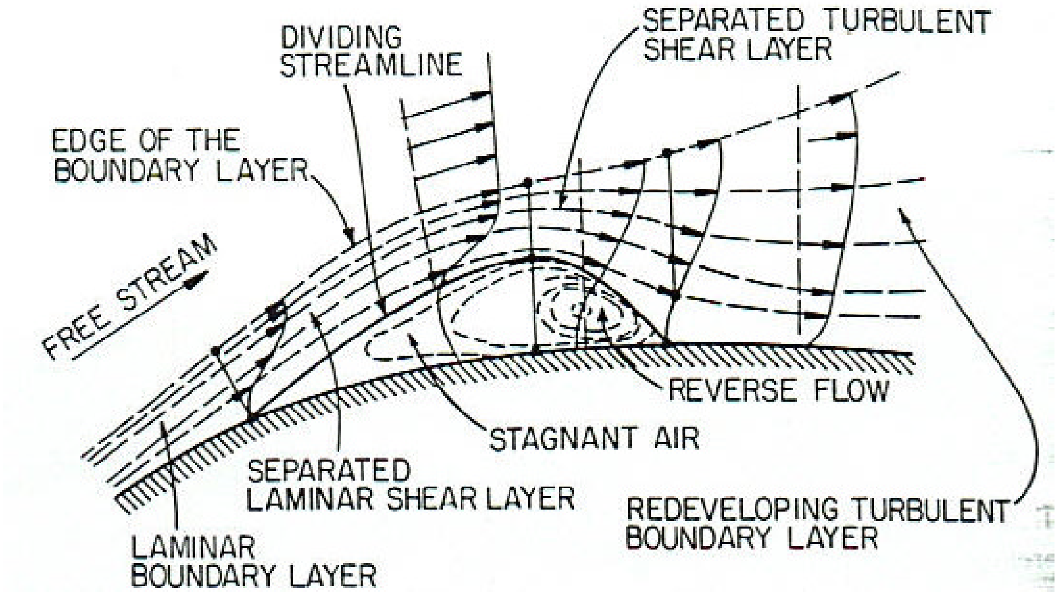


**Figure 2.1 Nature of Laminar Separation Bubble on a Turbine Blade**

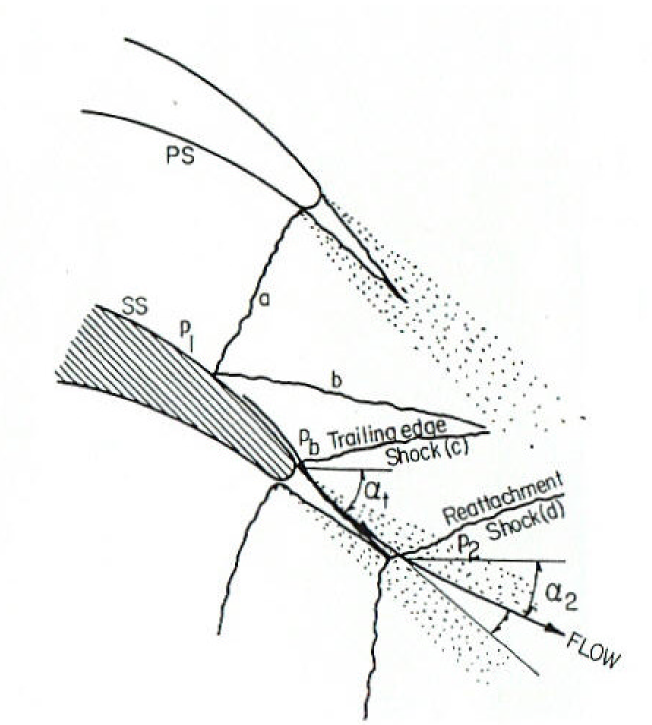


**Figure 2.2 Trailing Edge Shock Structure**

growth. The viscous layer near the shock impingement point has to gain momentum to overcome the pressure rise in that region. Interacting with free stream, the viscous layer increases it's momentum and thickness. This growth will lead to localized boundary layer separation. After the incident shock, the boundary layer will reattach as the flow is encountering a favorable pressure and it's still accelerating. A detailed picture of trailing edge shock structure is shown in Figure 2.2.

## 2.3 Loss Mechanisms

Modern day turbines are designed to generate huge power output. This is achieved by increasing the Mach number of the inlet flow at each stage substantially, which is to increase the load on the blades. Due to the presence of strong flow acceleration the total loss in a turbine is increased. Losses are manifested in the form of viscous dissipation and are represented by stagnation pressure loss. Evidenced by the following equation, viscous dissipation increases entropy and is unable to perform useful work.

$$\frac{\Delta s}{R} = -\ln\frac{P_{o2}}{P_{o1}} = -\ln\left[1 - \frac{(\Delta P_o)_{loss}}{P_{o1}}\right] \qquad (2.1)$$

The overall losses in a steam turbine is a composition of various losses such as profile loss, secondary loss, annulus loss, and tip clearance loss. In cascade tests, some of these losses are omitted due the inherent setup of the cascade. When handling losses measured in a cascade test, profile loss is of primary importance and it is a function of parameters such as, incidence, solidity, trailing edge thickness, curvature of surface near trailing edge, surface roughness, Mach number and Reynold's number. The breakdown for the total loss in a cascade test is as follow,

i) Profile loss associated with boundary layer growth.
ii) Shock loss arising from normal or oblique shocks at trailing edge.

iii) Mixing loss due to rapid dissipation of the wake and shock-boundary layer interaction.

At subsonic exit flows, profile loss coupled with mixing loss are the main components accounting for the total loss. Friction increases entropy and internal energy of the boundary layer while losing stagnation pressure. As the flow exits the trailing edge of the blades, the wake interacts rapidly with the free stream. Eventually at some point downstream of the blades, the flow will be completely mixed out exhibiting a uniform velocity profile.

Transonic exit flows are associated with higher overall losses when shock waves start to form at the trailing edges. This form of loss is attributed to Mach number effects. The initial formation of weak normal shocks has negligible effect on the shock loss and the exit flow has a sub-unity Mach number. Significant shock losses are recorded when the exit flow Mach number exceeds unity (Lakshminarayana, 1996). When the exit Mach number increases, the formation of shocks will move downstream on the suction surface and the shock structure changes from normal to oblique. The loss estimated from shocks and their interaction with the boundary layer surpass losses due to viscous effect by the boundary layer alone. Hence at high Mach numbers, shock loss and shock-boundary layer interaction loss are the key components attributing to the total loss. In most instances, the total loss can increase by 100% at Mach numbers exceeding unity. Mee et al. (1990) recorded loss associated with trailing edge shock, wake mixing and flow separation accounting between 30-70% of the total loss.

### 2.3.1 Effect of Incidence

The primary focus of this investigation is the effect of incidence on the total loss. Turbine blades are usually designed to perform at optimum level when the flow approaching is at design condition, zero to the leading edge. However, some blades in industry are designed to perform at off-incidence, which means the design incidence has a value other than zero.  Incidence arises when the turbine is required to operate at off-design conditions such as idling, variable speed and varying loading.  In steam turbine terminology, incidence is defined as the difference between the inlet blade angle and the inlet flow angle.  All angles are measured with the respect to the tangential plane at the leading edge.  For gas turbines, the angles are measured from the axial plane.  The effects of incidence on the total loss vary with different blade profile and geometry.  Incidence loss is strongly affected by the leading edge geometry, the nose shape will determine the possibility and extent of flow separation (Chen, 1987).  The exit flow angle is however unaffected by incidence and the turning angle remains constant.  Total loss will hence increase as incidence is increased or decreased.  Certain blade profiles have the capability of maintaining constant loss at a ten-degree incidence range while there are others that demonstrate steep increase in losses when operating at off-design incidence.  Figure 2.3 shows the trend of profile loss against the variation of incidence for impulse and reaction turbine blades used in the 1950's (Ainley, 1948).

Most turbine blade passages are either convergent or convergent-divergent.  When flow approaches the leading edge at off-design incidence, it is strongly accelerated around the nose.  Once reaching the pressure or suction surface, the flow will be decelerated and then accelerated again.  Due to passage convergence, turbine blades can withstand a range incidence without significant increase in losses.

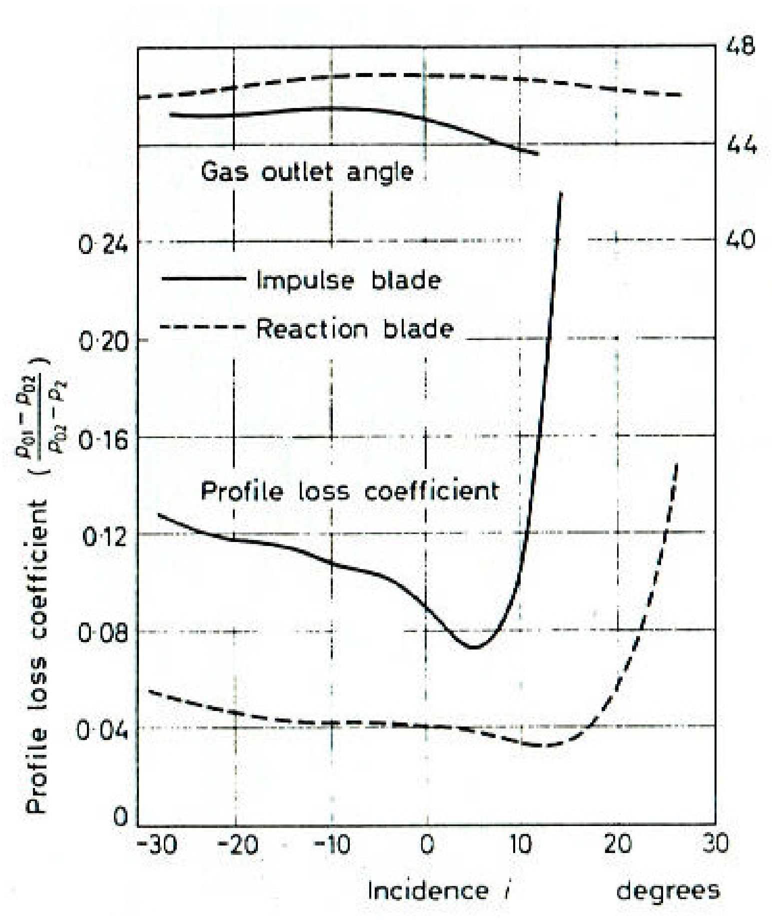


**Figure 2.3 Variation of Profile Loss with Incidence**

## 2.4 Previous Research

Cascade tests are commonly performed to evaluate the aerodynamic losses of turbine blades. Published cascade data for steam turbine blades tested at transonic exit Mach numbers with incidence are however limited. In late eighties, Hodson and Dominy (1987), Goobie et al. (1989), and Venkatrayulu et al. (1989) published articles demonstrating the effect of incidence on the performance of the turbine rotor blades.

Goobie et al. (1989) performed cascade test for a large scale, low-speed axial turbine rotor blade. Losses are measured at $-15^o$, $0^o$ and, $15^o$ of incidence with zero incidence as the design flow incidence. The turning angle was 93.2 degree and the aspect ratio is 1.23. Traverses are made at four different exit planes 20%-174% of the axial chord. The measured losses at these four planes are almost identical at design incidence.
This effect can be accounted by low momentum exit flow with low subsonic Mach numbers. At off-design incidence, profile loss is shown to increase. At the positive incidence, the loss is the highest among the three incident angle tested. Surface pressure measurement has documented the possible formation of leading edge separation bubble. Overall this particular turbine blade has demonstrated to be tolerant to negative flow incidence and is suitable for operation at range of negative incidence without any steep increase in losses.

Hodson and Dominy (1987), explored the effect of incidence, Reynold’s number, and pitch-chord ratio on the 3-D performance of a low pressure turbine cascade. Cascade tests are performed at incidence ranging $-20^o$ to $9^o$. The Mach number at the exit can be varied independently of the Reynold’s number. It is noted that with the increase of Reynold’s numbers at design incidence the profile loss decreased. At some instances, the profile loss decreased by 25% when the Reynold’s number is quadrupled. At a high Reynold’s number of $6.0 \times 10^5$, the flow is turbulent enough to keep the boundary layer attached to the blade. With the aid of surface pressure measurement, Hodson and Dominy (1987) clearly showed that positive incidence will cause separation bubbles to be formed near the trailing edge of the blade. At positive incidence, the blade loading is increased causing a region of adverse pressure gradient to be formed on the suction surface and the three-dimensional end wall flow is more dominant. Spanwise aerodynamic measurements did confirm that the secondary flow is evidently nearer to the mid-span for positive incidence. Aside from the end wall flow perturbation, flow on the blade surface is mostly two-dimensional along the span. Profile loss is almost constant for 40% of the span. Turbine cascade of low aspect ratio will have their mid-span profile loss influenced by secondary flow at the end walls. Profile loss is lowest at the design incidence with the loss increasing with incidence (Hodson and Dominy, 1987).

Venkataryulu et al. (1989) tested a set of 50% reaction turbine blade at three incidences of $-16^{o}$, $0^{o}$, and $14^{o}$ in a Mach number range of 0.3 to 0.86. The design Mach number for this set of rotor blades is 0.75. Like Hodson and Dominy (1987), flow separation is expected to happen near the trailing edge due to adverse pressure gradient at that region. The loss measurement from Venkataryulu et al. (1989) are presented using pressure loss and kinetic energy loss coefficients. The trends of these two loss coefficients varied with exit Mach number are quite similar. Total loss appeared to decay from Mach 0.3 to the critical Mach number due to the decrease in viscous effects at higher Mach numbers. At Mach number exceeding the critical Mach number, the total loss increased steeply due to the addition of shock loss and the shock-boundary layer interaction loss (Venkataryulu et al., 1989). Like the previous two researches reported above (Goobie and Hodson), the measured loss by Venkataryulu is highest at positive incidence that is in this case at $14^{o}$.

## 2.5 Prediction Methods

Implementing loss prediction methods is essential in blade design. Since the 1950's extensive research has been performed in loss prediction methods for turbines. Pioneers such as Ainley and Mathieson (1951) created a profile loss correlation that is dependent on blade geometry, flow and blade angles. The off-design loss is expressed in terms of the positive stalling incidence and zero incidence profile loss. This prediction method is suitable for exit flow with Mach number lesser than 0.6. The assumptions made at that time are the profile loss is independent of the exit Mach number, and the exit flow angle is unaffected by variation of incidence.

Thirty years later Kacker and Okapuu (1981) refined the prediction methods by Ainley and Mathieson (1951) to include loss resulting from shock formation and channel acceleration. Cascade tests performed at higher exit Mach numbers have demonstrated increased in total loss which cannot be accounted by the loss prediction from Ainley Mathieson (1951). A proportionality constant is also factored into the overall loss calculation to match up with advancement in the design of blade profiles over the three decades. The total loss is defined as,

$$Y_P = 0.914\left(\frac{2}{3} Y_{P,AMDC} K_p * Y_{shock}\right) \qquad (2.2)$$

This loss system is applied to 33 sets of turbine cascade data and is capable of predicting efficiency within ± 1.5 efficiency points.

More recently, Chen (1987) presented a method for predicting energy losses for transonic low-pressure steam turbine blades. Fifty sets of cascade test data obtained for exit Mach number ranging from 0.8 to 1.6 are used to formulate the loss model. Chen (1987) adopted the basic loss model from Craig and Cox (1971) and improved the loss prediction system to accommodate the effects of Mach number in transonic flow. Studies made at the hub, mean and tip section showed that the loss coefficient peaked between Mach 0.9 to 1.1. This is due to the formation of normal shocks at that Mach number range and the interaction with the boundary layer. The normal shocks later turn into weak oblique shocks and as the Mach number is further increased, stronger oblique shocks developed which give rise to loss increase. The profile loss coefficients generated from the prediction method by Kacker and Okapuu will be compared with test results from the current experiments in chapter four.

# Chapter 3 EXPERIMENTAL METHODS

The following chapter describes the blades used in the cascade test, the testing facilities, setup of the cascade, and data reduction techniques.

## 3.1 Wind Tunnel Facility

The wind tunnel in Virginia Tech is a blow-down type facility. A four-stage reciprocating compressor is used to pressurize air in storage tanks. A power control panel located in the laboratory is used to control the storage tank pressures and to activate the blow-down sequence. Upon discharge from the storage tanks, the cool air passes through an activated-alumina dryer to de-humidify the air. Safety valve and control valve is used to maintain constant total pressure upstream of the test-section. Flow in the duct upon entering the test-section is straightened via flow straighteners and a mesh-wired frame is installed to provide uniform flow. Before each run, the control valve is activated to open at a certain angle. This pneumatically controlled valve is fed with pressurized air at 20 psig. When the tunnel is started this butterfly valve will automatically adjust itself to main constant mass flow and total pressure as specified by tunnel control computer. Typically the valve takes 5 seconds to achieve constant upstream pressure and is able maintain constant mass flow rate for 15 seconds. Figure 3.1 shows the structure of Virginia Tech's blow-down wind tunnel facility.

## 3.2 The Test-section Used

The design and shape of the test-section can affect aerodynamic measurements made in a cascade. Flow guidance at the exit plane is quite important. The transonic test-section built for cascade test is ideal for flow with zero inlet angle. Good periodicity in exit flow is possible for moderate turning.

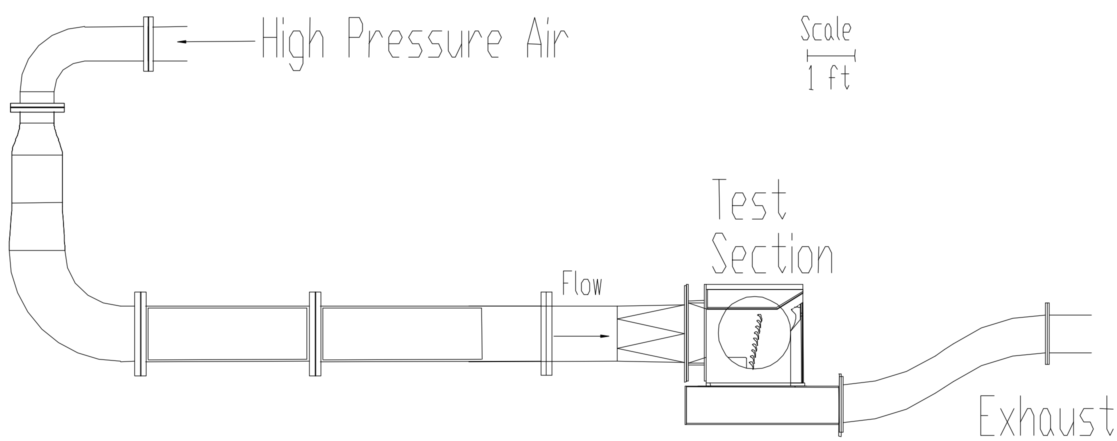


**Figure 3.1 Blow-down Wind Tunnel**

When the turning angle increased, the flow will have difficulty in maintaining constant flow properties and flow periodicity at the exit plane of the blades.  A picture of the test-section used in the experiments is shown in Figure 3.2.  Aluminum blocks located around the cascade guide the flow at the inlet and exit of the test-section.  The inlet blocks ensure that flow is parallel at the inlet of the cascade.  The cascaded blades are mounted on circular plexiglass(one inch thick) with a dowel pin and a hex screw.  This fixture is then mounted onto the test-section with external aluminum plates and clamps for sturdiness.  Using an alignment pin fixed onto the test-section, the cascade can be rotated to achieve various inlet flow incidences.  The current setup allows the cascade to be rotated from $-45^o$ to $50^o$.  A probe traverse driven by a 10 watts stepper motor is utilized to make pressure measurements at various exit planes of the cascade.  It is mounted onto the exhaust structure where slots on the bottom of the exhaust allow the probe movement.

### 3.2.1 The Nozzles Studied

Two sets of nozzles used in the high-pressure stage of steam turbines were tested using the current transonic test-section.  The profile of these two nozzles is distinctively different.  However, both sets of blades seem to have a rather flat suction side curvature at the trailing edge.  Regardless of their difference in profile, both blades exhibit flow geometry that is quite similar to each other.  The inlet blade angles for the nozzles are $75^o$ and $85^o$ respectively.  The exit flow angle is $12^o$ for both blades.  In addition both nozzles are designed to operate at Mach 0.5.  Figure 3.3 displays the dimension of the nozzles and their respective profiles.  Since these nozzles are used in the high-pressure stage they are generally shorter in length than their counterparts fixed at the later stages of the turbine.  The nozzles used for the cascade test are all six inches in span.  Nozzles are oftenly replicated at the high pressure stages without change in their basic profile.  The nozzles are two-dimensional in profile and in cascade tests, the flow entering the entire span of the nozzles have constant properties.  This is not true in the stages observed in a real multistage steam turbine.  In multistage turbines, rotors with twist along the span will

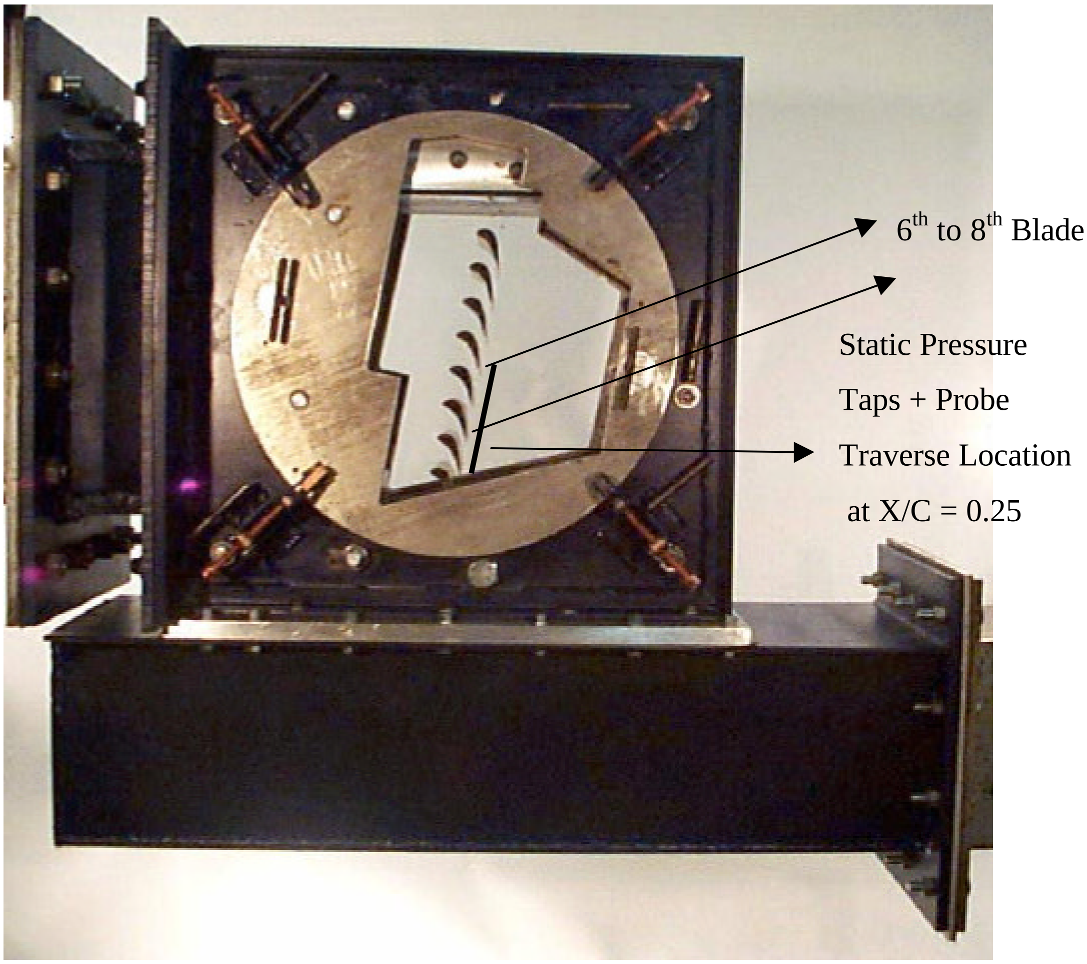


**Figure 3.2 Instrumented Test-Section**

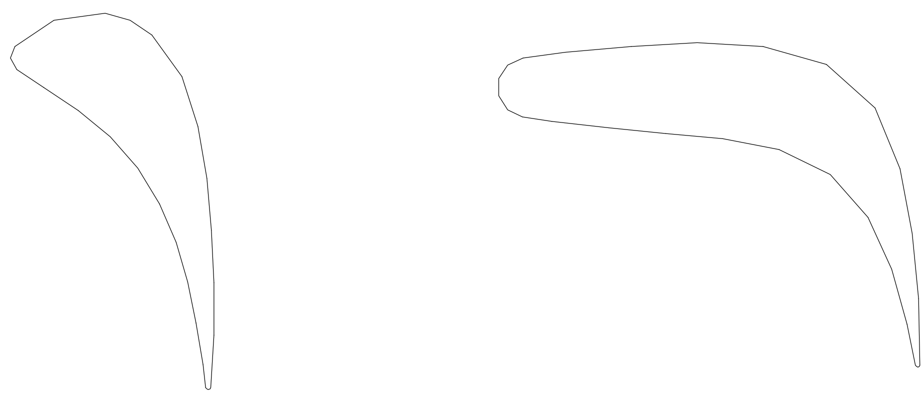

**526A** **525B**

**Figure 3.3 Blade Profiles of Tested Nozzles**

**Table 3.1  Blade Specification**

| Type | 526A | 525B |
|---|---|---|
| Chord (in) | 2.01 | 2.58 |
| Pitch (in) | 1.5 | 1.2 |
| Inlet Blade Angle,$\beta_1$ | $76.4^o$ | $85^o$ |
| Exit Flow Angle, $\alpha_2$ | $11.54^o$ | $12^o$ |
| Solidity (c/s) | 1.34 | 2.15 |
| Gauging (o/s) | 0.2 | 0.2 |

generate different exit conditions. Hence, the subsequent stage of nozzles will experience different flow along the span. The leading edge of the two sets of nozzles determines the possibility and extent of flow separation when the inlet flow approaches the leading edge at an incident angle. Positive incidence normally results in separation at the leading edge of the suction surface, coupled with stronger blade loading the chances of flow separation is much higher than flow entering at negative incidence. At negative incidence, the flow may separate at the leading edge of the pressure side and will eventually reattach near the trailing edge as flow acceleration is more pronounced in that region. Since one nozzle has a longer axial width than the other translates to a larger surface area, it is expected that its profile loss will be greater than the other nozzle.

It’s imperative for blade designers to decide on the number of blades used in each nozzle stage. The spacing between adjacent blades has to be optimal to effectively control frictional losses. Blade solidity is determined by the ratio of the blade’s chord and blade spacing otherwise known as pitch. The solidity for the nozzle Type 526A is 1.33 and 2.15 for Type 525B. High solidity causes higher viscous losses due to the proximity between adjacent blades. On the other hand, low solidity induces flow separation for incidental inlet flow. Early turbine designers used a criterion based on non-dimensional force in the cascade by Zwifel to obtain the optimum blade solidity. Previous studies on the effects of blade solidity have concluded that any deviance from the design value will lead to steep increase of losses.

Figure 3.4 illustrates the essential parameters used in defining blade geometries. Other than flow and blade inlet and exit angles, non-dimensional parameters such as gauging (throat/pitch) and aspect ratio(span/chord) affects the measured losses. Aspect ratio determines the influence of secondary flow on the flow at the mid-span. Blades of low aspect ratio have three-dimensional flow covering a sizeable portion of the span. This type of flow causes the measured losses at mid-span to increase.

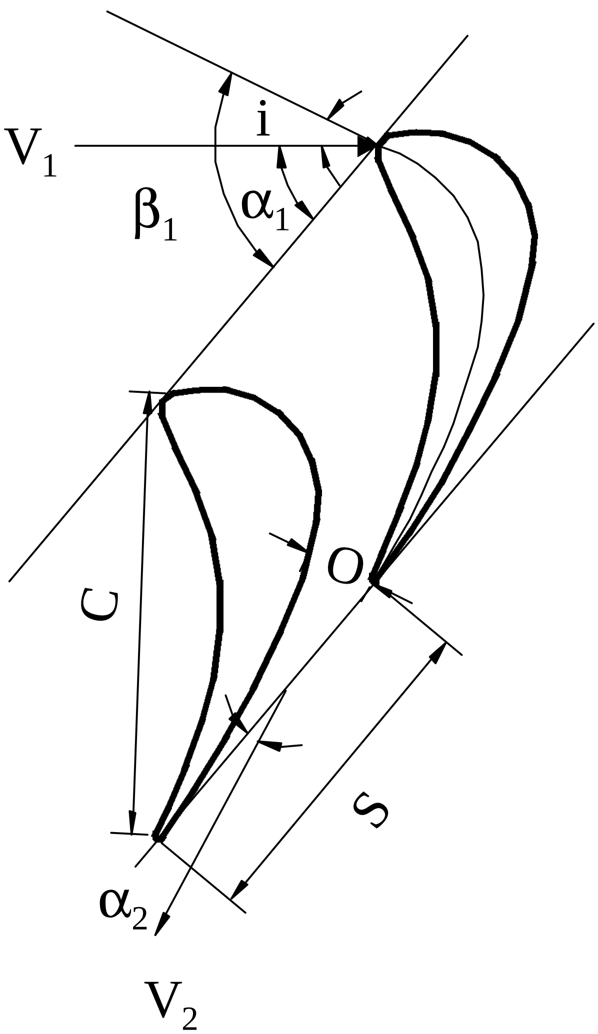


**Figure 3.4 Nomenclature of Blade Geometry**

### 3.3 Instrumentation and Data Acquisition

Aerodynamic measurements are made to obtain data to investigate the variation of losses with different incidence. The cascade is mainly instrumented to perform pressure measurements. Upstream total pressure measurement is conducted using a stationary Pitot probe positioned at approximately one foot ahead of the test-section. The upstream total pressure is relatively constant to the leading edge plane of the cascade as documented from previous studies.

A probe traverse is mounted at 0.5 inch from the exit plane of the cascade to obtain downstream pressure data. The probe is angled at the designed exit flow angle of the cascade. Even if there is exit flow deviation, this flat nose Pitot probe is accurate in measuring at $\pm 20^{o}$ deviation in angle from the probe's fixed position. The downstream probe is tasked to traverse two blade passages at the rate of six seconds per pitch driven by a RAPIDSYN stepper motor. A simple program has been written to control the step size for the probe.

Static pressure measurements are made by mounting static taps on the walls of the test-section. A Pitot-static probe is not used as it is inefficient in measuring static pressures in transonic flow. The size of the static holes is 1/32 inches in diameter and they are spaced at 0.2-0.3 inches intervals. Each blade passage contains 6-7 pressure taps. The locations of the static holes are aligned along the plane of the probe traverse. Four static pressure taps are also mounted upstream of the cascade to obtain the upstream static pressure and to verify the constant inlet flow between passages.

In addition, a relative humidity sensor is positioned upstream of cascade together with a type-K thermocouple. Upstream temperature readings are essential as they are used later for data reduction to arrive at the computed losses. The effects of relative humidity on aerodynamic measurements have been studied previously. Total loss increases with high relative humidity. The acceptable relative humidity level for this experiment is set to be 10 percent.

Data acquisition for each tunnel run is performed a high data acquisition system (LeCroy) and a independent pressure measurement system. The LeCroy is capable of acquiring data from eight channels at a time. The acquisition rate for each run is fixed at 50 cycles per second. Data obtained by the LeCroy are the upstream total pressure and total temperature, differential pressure between upstream and the probe, and the displacement of the traverse. A simple low-pass RC filter is used for filtering signals from the differential pressure.

The upstream total pressure is measured using a single channel absolute pressure transducer capable of measuring pressure from 0-100 psi. A differential pressure transducer is then used to measure the pressure difference between the upstream total pressure and the probe's total pressure. The downstream total pressure is then obtained by the subtracting the differential from the upstream total pressure. The pressure transducers are calibrated periodically using an AMETEK deadweight tester. The deadweights are categorized in terms of gage pressure. Each calibration consists of obtaining 6 voltage outputs from pressure ranging from 0-30 psig. A linear line is fitted to the calibrated points using least squares approximation.

Static pressure measurement is performed using a self-calibrated and independent pressure measurement system (PSI). This system obtains pressure readouts via a 32 channel pressure transducer. Before data acquisition, the system calibrates itself using 2 reference pressure at 0 and 100 psig and generate a calibration curve. This allows sub-atmospheric pressure measurements to be conducted. After acquiring data, the voltage sensed by the transducer is forwarded to a math processor in the system that eventually provides gage pressure outputs.

Each tunnel run has a standard time of approximately 25 seconds. Data is acquired after 5 seconds for the upstream pressure to stabilize. The data acquisition system is set for collecting data with 20 seconds period and 1000 points of data are collected at each tunnel run. The pressure measurement system is then set to collect data as soon as the

LeCroy is triggered manually. Usually, the total time taken for the probe to traverse two blade passages is 12 seconds. PSI is then set to collect 10 sets of data within that 12 seconds. Each measurement set consists of the average value of 10 frames of data taken in 1 second. The delay time between all measurement is set to be 0.22 seconds. The delay time between triggering the system and the first measurement set is less than a millisecond. A schematic diagram of the data acquisition procedure is displayed in Figure 3.5.

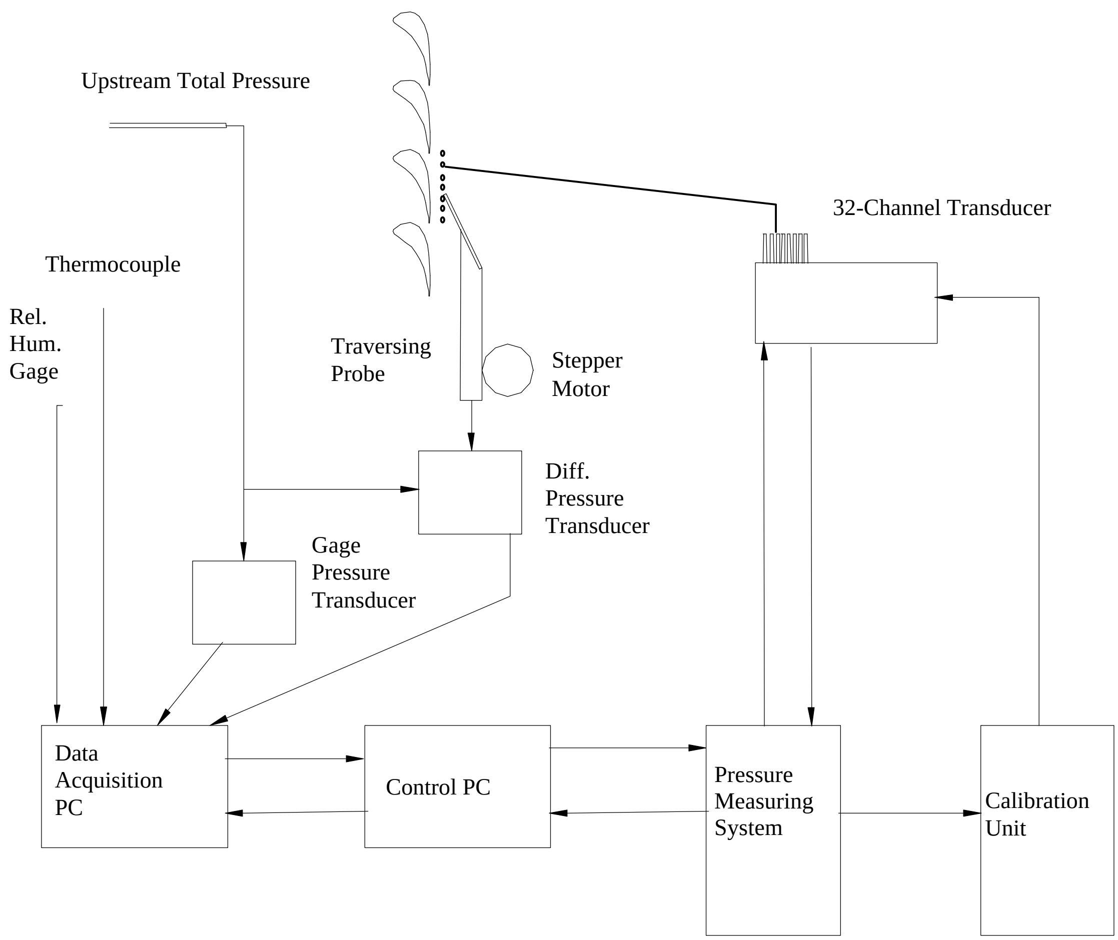


**Figure 3.5 Schematic Diagram for Data Acquisition**

### 3.3.1 Shadowgraph and Schlieren Photography

Shadow and schlieren photography are two flow visualization techniques that are essential to investigate flow in the cascade. Being easier to setup among the two methods, shadow photography is more commonly used to obtain photographs of flow fields in this cascade. The main characteristic of this method is that the difference in density of the image is proportional to the derivative of gradient in refractive index in the field. Using a nanopulser as a light source and a parabolic mirror of 80 inch focal length, shadowgraphs are relatively easily to produce. Figure 3.6 shows the setup to perform shadow photography. Parallel light rays reflecting from the parabolic mirror is passed through the cascade and the image is captured on a Polaroid type 57 film.

Schlieren photography requires a more extensive setup than shadow photography. This method indicates the gradient in refractive index in the flow field. Shadow photography requires flow strong gradients to attain good results but pictures obtained from schlieren technique showed finer sensitivity to changes in temperature and the difference can be as small as $10^{o}$ Fahrenheit. However, the schlieren setup for the cascade tested at VPI produced mediocre results compared to the shadowgraphs.

### 3.3.2 Color Surface Oil Flow Visualization

Another method of visualizing flow in a cascade is to coat the cascade with a mixture of dye and oil. Flow field in the cascade is investigated after the tunnel is ran for a certain exit Mach number. The pattern formed by the mixture on the blades and end walls is used to interpret flow behavior. Oil flow visualization is extremely helpful in investigating the effects of secondary flow in the cascade. In addition it clearly displays discontinuities such as flow separation and shock location. This form of flow visualization also aids in explaining flow data obtained through aerodynamic measurements made in the cascade.

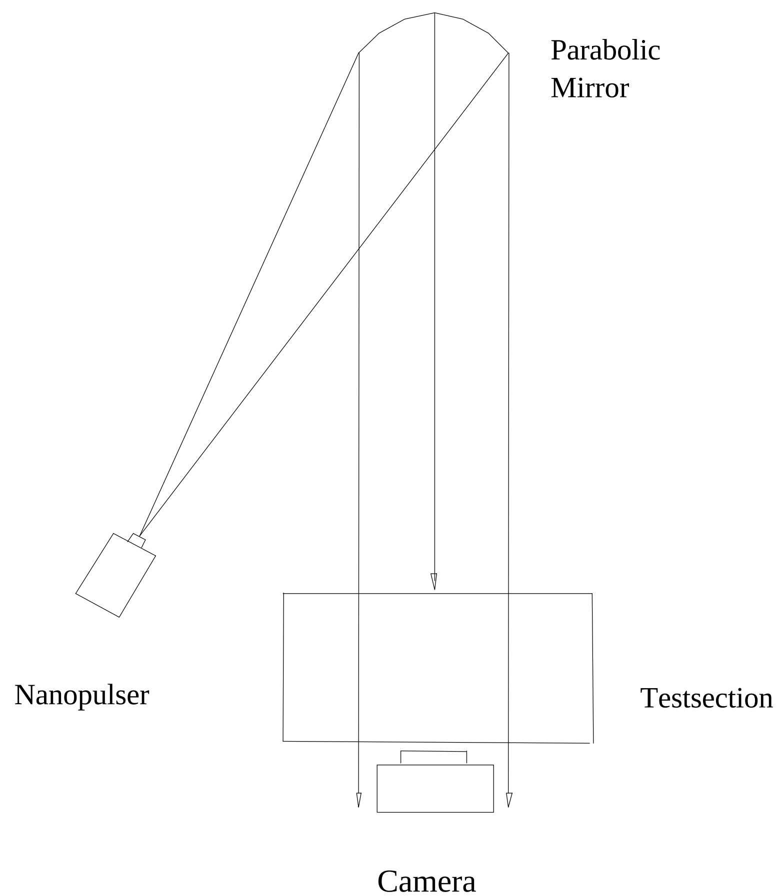


**Figure 3.6 Setup for Shadow Photography**

### 3.4 Data Reduction

The objective of this experiment is to investigate the effects of incidence on the loss coefficient. Two forms of loss coefficient are determined using the data obtained through aerodynamic measurement made in the blades passage between the 6th and 8th blade in the cascade. These loss coefficients are pressure loss coefficient and kinetic loss coefficient. Essentially, these loss coefficients are just different forms representing the loss coefficient. Loss coefficients are initially calculated for the individual passage. As the flow in the two blade passage is not exactly identical, an arithmetic averaged loss coefficient is calculated. Only 6-7 static pressure taps are installed in each blade passage for the two sets of nozzles tested. Hence, the downstream total pressure readouts obtained at the position of the wall static taps are used in determining the local loss coefficient and exit Mach number.

The mass-averaged form of the pressure loss coefficient and the kinetic loss coefficient over the two blade pitches are displayed in equation 3.1 and 3.2 respectively.

$$\omega = \left[ \frac{\int ((P_{o1} - P_{o2}) / P_{o1}) \rho_2 V_2 dy}{\int \rho_2 V_2 dy} \right] \tag{3.1}$$

$$\tau = \left[ \frac{\int (1 - (V_2 / V_{2i})^2) \rho_2 V_2 dy}{\int \rho_2 V_2 dy} \right] \tag{3.2}$$

Static pressure readings at each location $p_{2j}$ obtained from the 12 seconds data acquisition time is averaged to arrive at a time independent static pressure reading $p_{2ja}$. The subscript represents the location of the static taps and the probe traverse along the exit tangential plane. This form of average is acceptable, as the variation in static pressure reading over time isn’t significant.

Upon matching the averaged the static pressure at each wall tap with the downstream probe traverse pressure, the exit Mach number at the location is calculated using the following equation

$$\frac{P_{o2j}}{p_{2j}} = \left(1 + \frac{\gamma - 1}{2} M_{2j}^{\ 2}\right)^{\frac{\gamma}{\gamma - 1}} \tag{3.3}$$

When evaluating the isentropic Mach number an equation similar to 3.3 is used except that the term $P_{o2j}$ is replaced by $P_{o1}$.

From the measured upstream total temperature, the downstream static pressure is evaluated using equation 3.4 assuming that the stagnation temperature $T_{o2}$=$T_{o1}$.

$$\frac{T_{o2}}{T_{2j}} = 1 + \frac{\gamma - 1}{2} M_{2j}^{\ 2} \tag{3.4}$$

The local density at the wall pressure taps is determined by the ideal gas law that states that

$$\rho_j = \frac{p_{2j}}{RT_{2j}} \tag{3.5}$$

and the local exit velocity is determined by the speed of sound relation in equation (3.6)

$$V_{2j} = \frac{M_{2j}}{\sqrt{\gamma RT_{2j}}} \tag{3.6}$$

A correction formula is necessary to correct data obtained when the probe traverse experiences supersonic flows or when the following condition is met.

$$\frac{P_{2j}}{P_{o1}} < 0.528 \tag{3.7}$$

With conditions mentioned above a bow shock is formed at the nose of the probe. The pressure measured by the probe is not representative of flow behavior at that point due to the presence of the bow shock. Rayleigh supersonic Pitot tube formula is used to correct the calculated exit Mach number and the measured pressure.

$$\frac{P_{o2j}}{P_{2j}} = \left(\frac{\gamma+1}{2} M_{2j}^{\ 2}\right)^{\frac{\gamma}{\gamma-1}} \Bigg/ \left(\frac{2\gamma}{\gamma+1} M_{2j}^{\ 2} - \frac{\gamma-1}{\gamma+1}\right)^{\frac{1}{\gamma-1}} \tag{3.8}$$

This formula is valid under the assumption that the wall static taps measure static pressure upstream of the bow shock. $M_{2j}$ is the corrected Mach number using the formula above. The corrected downstream total pressure is evaluated using equation 3.1 with the corrected Mach number. The exit density and velocity have to be determined too.

# CHAPTER 4  RESULTS AND DISCUSSION

In this chapter, the loss coefficient calculated from the measured pressure data will be discussed with variation in exit Mach number and flow incidence.  Comparing with available published data of turbine blades with similar profile and blade geometry will reaffirm the validity of the current experimental data.  The losses from the two nozzles tested will be compared.  In addition, a prediction method from Kacker and Okapuu is used to predict the losses for the nozzles tested.  A revised shock model is implemented to better account for the losses at transonic conditions.

## 4.1 Total Pressure Loss Measurements, Blade 526A

This section will cover the total pressure measurements and loss results for tested nozzle 526A.  Data presented included surface-oil-flow-visualization, total pressure ratio plots, and shadowgraphs.

### 4.1.1 Downstream Total Pressure Profiles

The measured downstream total pressure profile is normalized with the upstream total pressure to obtain the pressure ratio.  The pressure ratio plots are varied with the pitch that is non-dimensionlized by the traversed distance over the length of the blade passage. These pressure ratio plots display the patterns and periodicity of the flow in the wake and the freestream of two different blade passages. A picture of the endwall captured using color oil flow visualization is shown in Figure 4.1.  At this condition, where i=-4$^{o}$ and the exit Mach number is 0.6, Figure 4.1 clearly showed the periodicity of the exit flow. Figure 4.2 through 4.4 displayed the pressure ratio plots for incident angles -4$^{o}$, -34$^{o}$, and 26$^{o}$ at various exit Mach numbers.  From the five pressure ratio plots at -4$^{o}$ incidence (Fig 4.2), it is evident that the pressure ratios in the freestream and in the wake decreased with increasing exit Mach numbers.  The periodicity of the exit flow seems to be good up until exit Mach 0.9. At Mach number exceeding unity, the pressure ratio in the first measured blade passage is lower than the second measured blade passage. This is due to limitation of the current test-section that does not have exit guide plates to control the periodicity of the exit flow at high transonic Mach numbers.

At -34$^o$ incidence (Fig 4.3), the wake profile is not symmetrical about the wake center at subsonic exit Mach numbers. This is caused by the pressure side separation as shown by the schlieren picture in Figure 4.5. This trend changed as the exit Mach number approaches unity and normal shocks start to form at the trailing edge. As the exit Mach number is increased beyond unity, the freestream in between two blades is no longer evident on the pressure ratio plots. Stronger shocks have developed across the throat at the trailing edge of the blade originating from the pressure side and impinging onto the suction surface of the next blade.

Flow entering the blade passage at positive incidence of 26$^o$ has significant lower pressure ratio than at the other two incidences at similar exit Mach numbers (Fig 4.4). Even at subsonic exit Mach 0.66, there is a 1% loss in the freestream. The periodicity is not good as previous cases. This may due to a large turning angle of 118$^o$ and the lack of flow guidance at the exit of the blade rows. Shadowgraphs taken at various exit Mach number displayed by Figure 4.6 show the progress of shock development and shock induced flow separation to be the dominating factors in creating such low pressure ratios.

In summary, the periodicity of the flow is good at design incidence. However, the periodicity degraded at off-design incidence. The total pressure ratio plots provide an overview of what the loss trend is like before computing the loss coefficients. In the next section, total pressure loss coefficients are calculated and the effects of Mach number and flow incidence will be discussed in more detail.

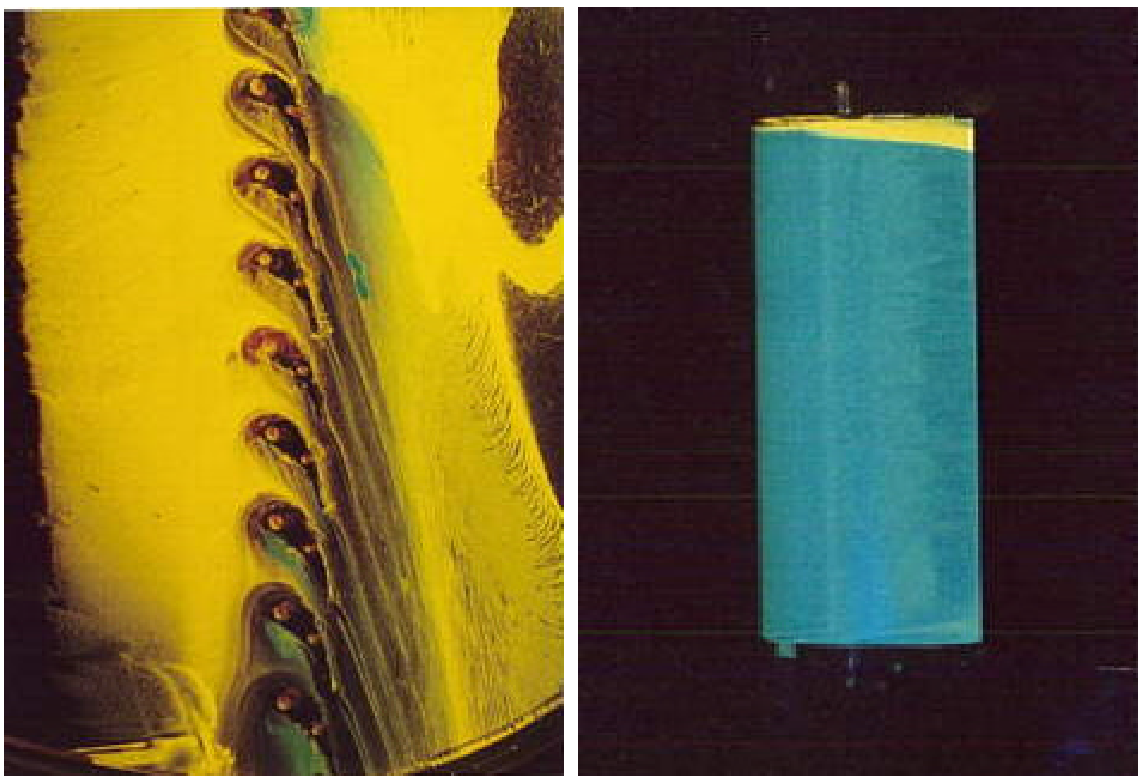

Endwall                                   Blade Suction Surface

**Figure 4.1 Color Oil Flow Visualization, i=-4$^{o}$, Mach=0.6**

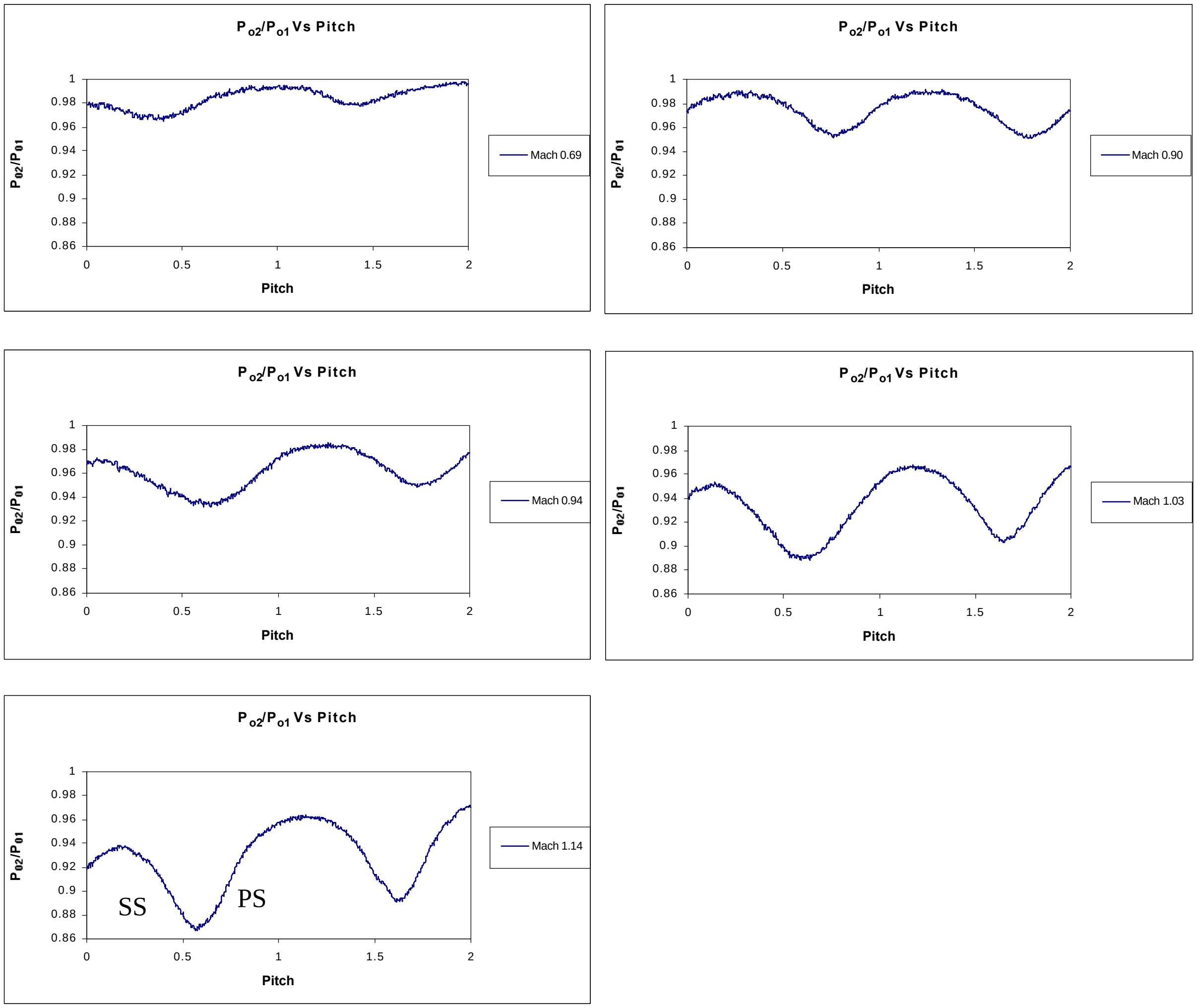


**Figure 4.2 Pressure Ratio at -4$^{o}$ Incidence**

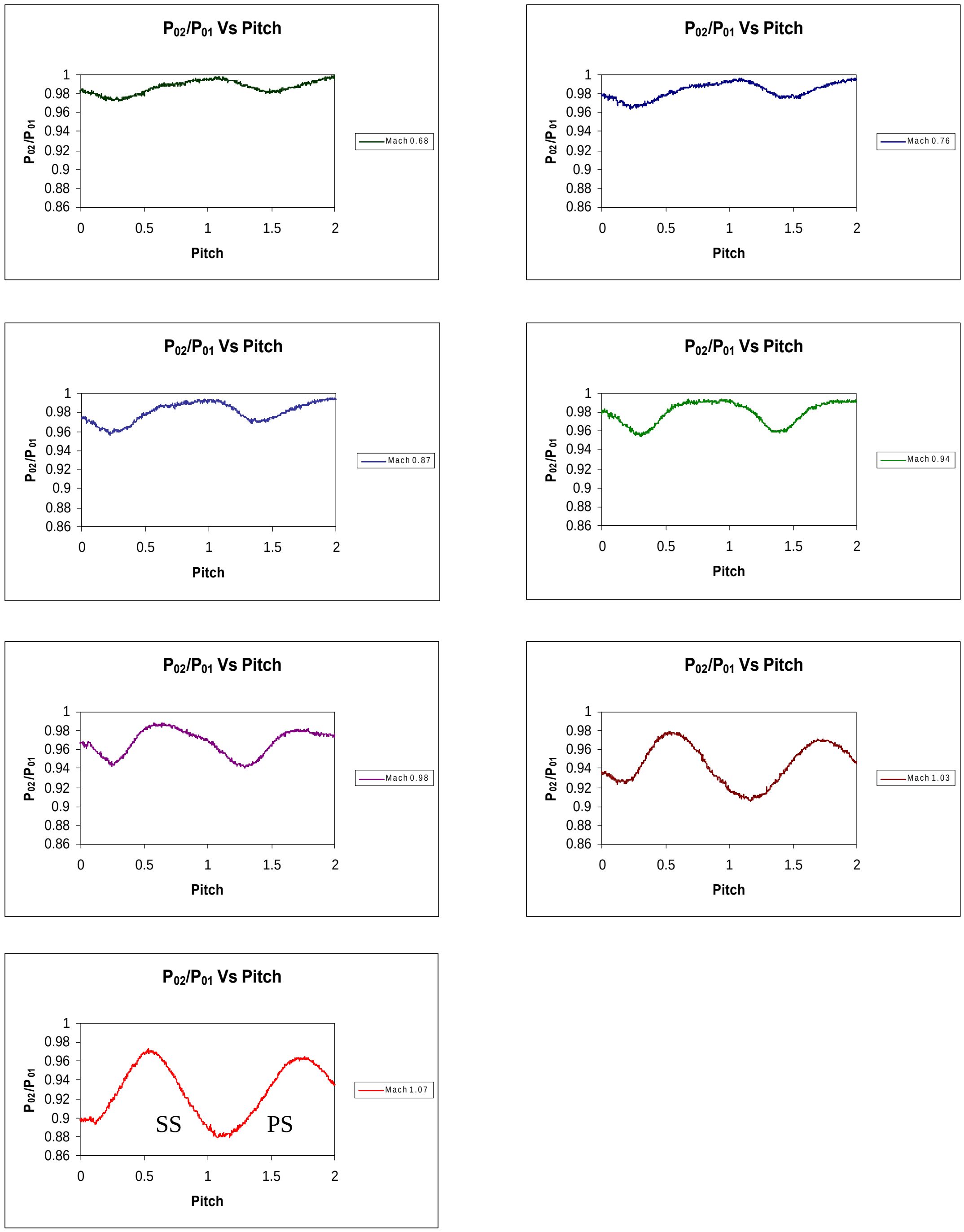


**Figure 4.3 Pressure Ratio at -34$^{o}$ Incidence**

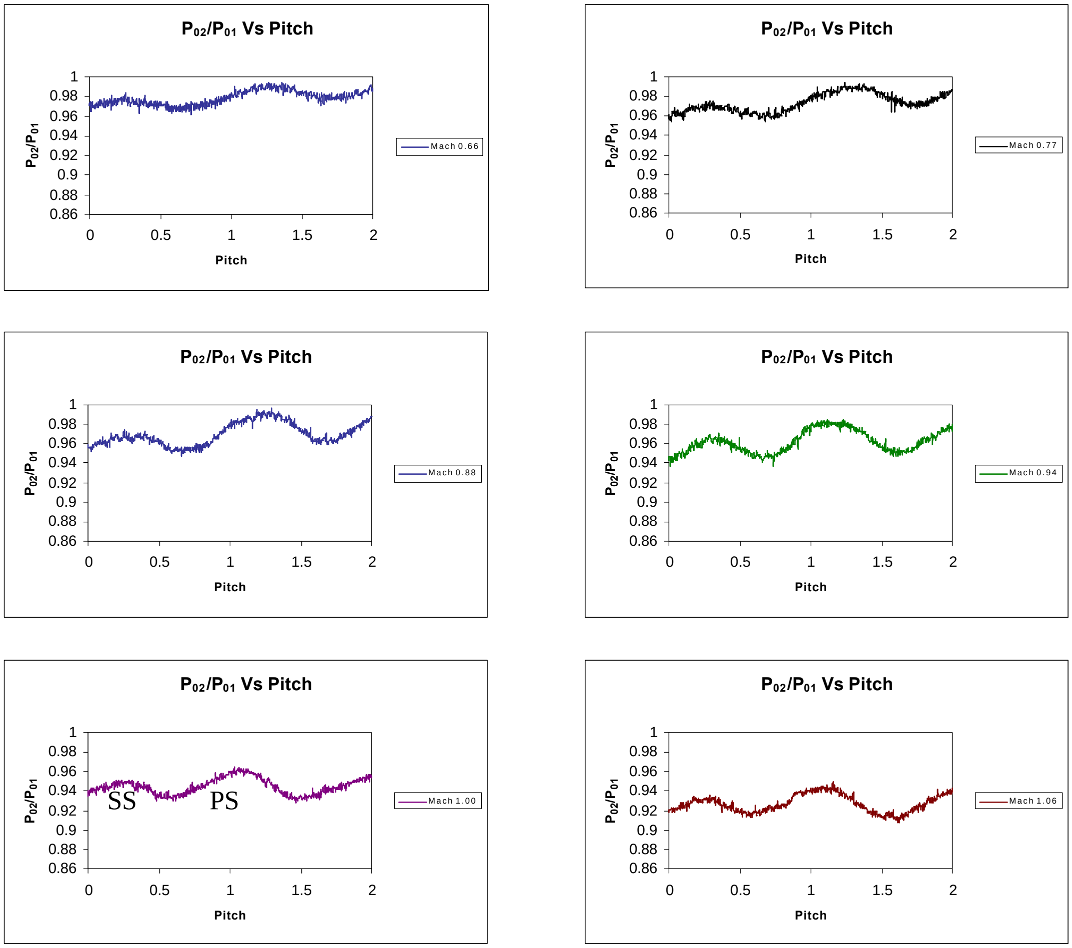


**Figure 4.4 Pressure Ratio at 26° Incidence**

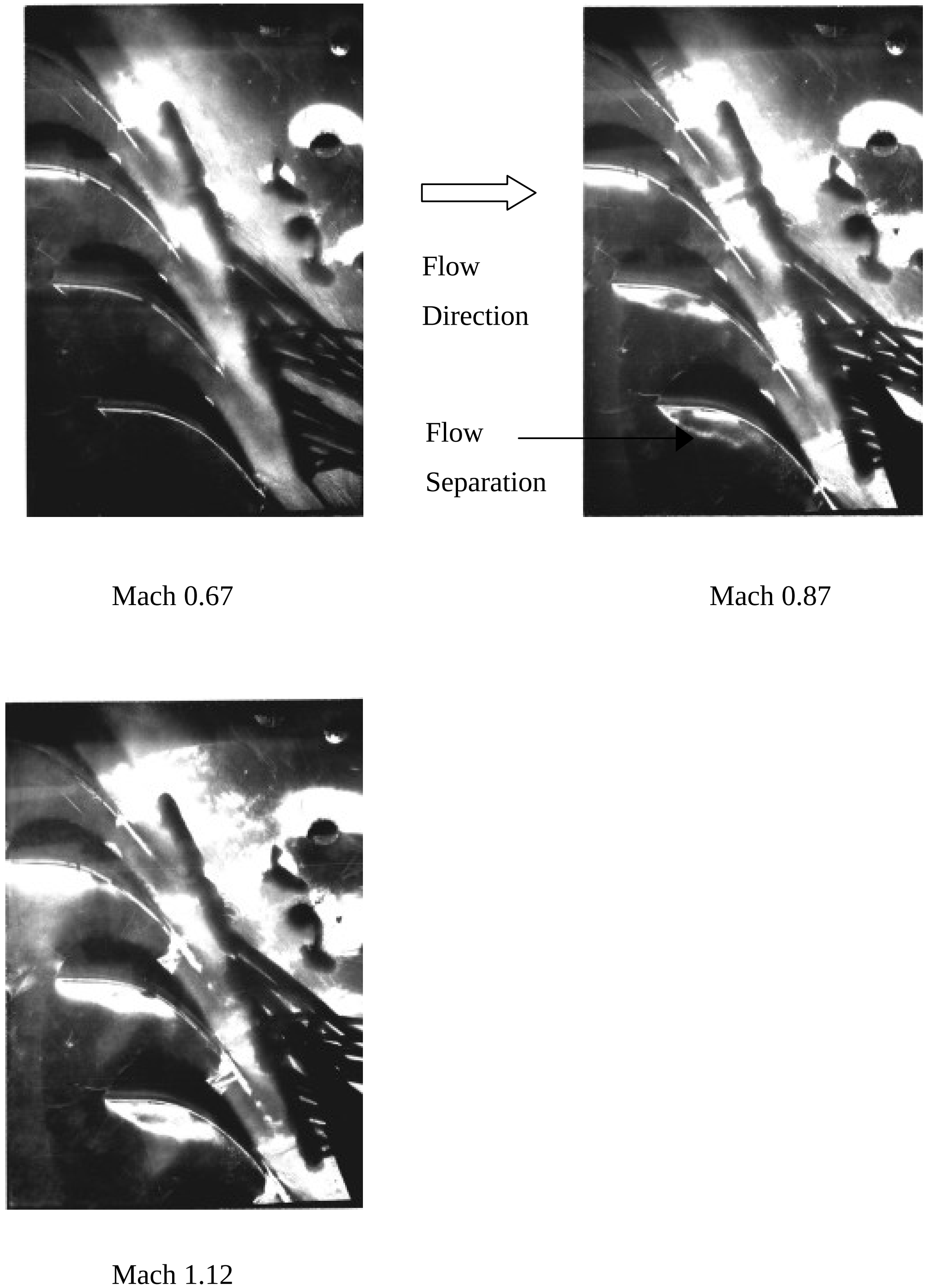


**Figure 4.5 Schlierens at -34° Incidence**

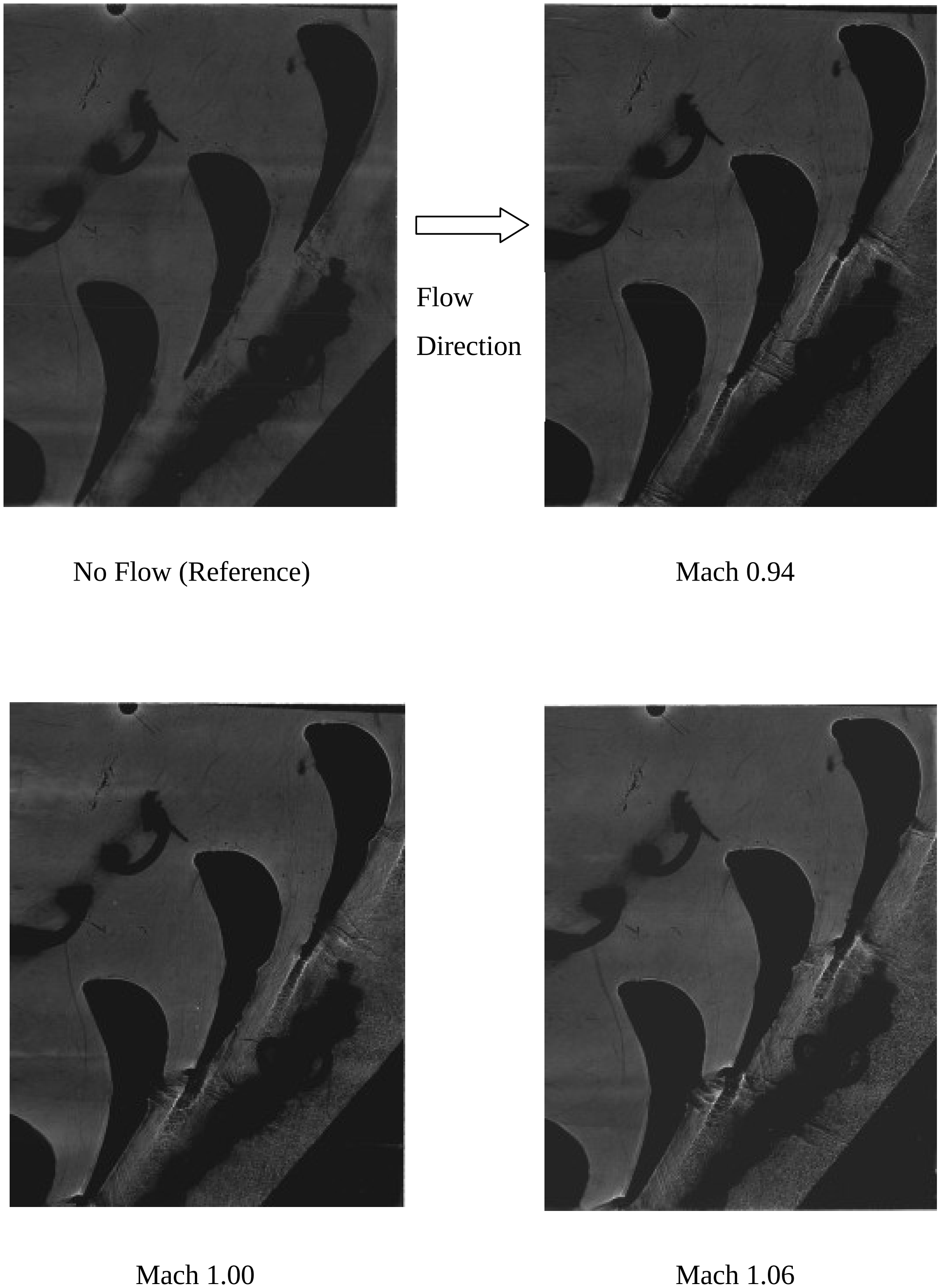


**Figure 4.6 Shadowgraphs at 26$^{o}$ Incidence**

### 4.1.2 Variation of Profile Loss with Mach Number and Incidence

With the measured pressure data, profile losses can be calculated into pressure loss coefficients and kinetic loss coefficients, as discussed in chapter three. Only the former will be presented in this particular section. Results in the form of kinetic loss are available in the appendix. The calculated mass-averaged pressure loss coefficients for the two measured blade passage are arithmetically averaged to arrive at a mean loss coefficient. The difference in loss coefficients between the two blade passages due to aperiodicity is expressed as an uncertainty band on the processed data. For simplicity, the pressure loss coefficient will be referred to as loss coefficient from here on. The loss coefficient plot with variation in exit Mach number is shown in Figure 4.7. The trend of the loss coefficient can be categorized into three regions. In subsonic flow at exit Mach below 0.90, the loss coefficient is dominated by viscous losses and losses are expected to be rather insensitive to exit Mach numbers. From Mach 0.90 to Mach 1.0, the presence of strong normal shocks causes the loss coefficient to increase at a steep gradient. This is referred to as the transonic region. When the normal shocks turned into weaker oblique shocks in supersonic flow, the loss coefficient will peak in the region of exit Mach 1.1-1.2 and subsequently decrease at higher Mach numbers until the formation of stronger oblique shocks. This is referred to as the supersonic region.

The trend of the loss coefficient variation with exit Mach number is quite similar at all three incident angles tested. Loss coefficients do not vary significantly with exit Mach number until exit Mach 0.95. At -4$^{o}$ incidence, the loss coefficient increased from 1.1% to 2.5% with exit Mach number from 0.69 to 0.90. This gradual increase is mostly due to higher viscous losses at higher exit Mach numbers as the blade passage is convergent. At subsequently higher exit Mach numbers, the loss coefficient increased steeply due to the formation of normal shocks at the trailing edge. The loss coefficient plateau at exit Mach 1.03 with a value of 6.1%. This suggests that the normal shocks are transforming into weaker oblique shocks justified by the loss coefficient at exit Mach 1.14 to be around

6%.  Mee et al. (1990) and Chen (1987) also observed the peak losses to occur between exit Mach 1.0 to 1.1.

The loss coefficients at -34$^o$ incidence behave closely to those at -4$^o$ incidence in subsonic exit flow.  It is indeed quite unusual for the losses at such extreme negative incidence to exhibit such resemblance to the losses at near design incidence.  Even though schlieren's pictures taken at high subsonic flow contained flow separation at the blade pressure surface with reattachment at 68% chord, it is not reflected on the loss coefficient.  The boundary layer on the suction surface is expected to remain laminar for most part of the surface under a favorable pressure gradient.  The pressure ratio plots from Figure 4.3 displayed periodic wake patterns as observed at -4$^o$ incidence.  In fact, the periodicity of the exit flow appears to look better at i=-34$^o$.  At exit Mach number 0.9 to 1.04, the loss coefficient for i=-34$^o$ is much lower than at near design (i=-4$^o$).  This is quite unusual as loss coefficient at extreme negative incidence is expected to exceed those at near design incidence.  From the pressure ratio plots in Figure 4.3 with exit Mach 0.87-0.98, the wake thickness is considerably smaller than the other angles.  There is also a distinctive presence of the freestream covering a larger exit area than the wake itself.  Possible explanation for this event would be the delay in shock formation due to the less favorable pressure gradient present and also due to underexpanded flow.  Once the exit Mach number is 1.07, the loss coefficient for i=-34$^o$ exceeds the loss coefficient at near design(i=-4$^o$).  Figure 4.5 displayed the presence on normal shocks appearing at the suction and pressure side of the trailing edge.  Together with the shock induced flow separation at the trailing edge, the normal shocks are major factors increasing the loss.  Due to limitation of the facility, no data are obtained at higher exit Mach numbers.  Hence, it cannot be concluded whether the loss coefficient will peak at this incidence.

Loss coefficients evaluated at 26$^o$ incidence possessed significantly higher losses than near design incidence in subsonic flow.  At exit Mach 0.66, the loss coefficient is 2% compared to 1.2% at -4$^o$ incidence.  This difference may be attributed to the possibly leading edge flow separation on the suction surface and the subsequent turbulent boundary layer formed after the reattachment.  Viscous losses are higher for a turbulent boundary layer than a laminar one. Since there is no region of adverse pressure gradient formed on the suction surface at -4$^{o}$ incidence, it is expected that a laminar boundary layer exists throughout the suction surface at subsonic exit flow. With flow entering the blade passage at extreme positive incidence, the blade loading is high causing a region of adverse pressure gradient to be formed on the suction surface. The losses at this incidence increased steeply starting from exit Mach 0.93. The loss coefficient increased to 8.6% at exit Mach 1.06 and does not seem to reach a maximum. Relatively, this loss is 18% greater than the loss computed at -4$^{o}$ incidence and 3% greater than the loss at -34$^{o}$ incidence. Trailing edge flow separation and shock-boundary layer interaction are the key components in escalating the loss at supersonic Mach numbers. Due to the facility limitation, no further data is obtained at higher Mach numbers. It is inconclusive about the trend of the loss coefficient beyond Mach 1.06 for i=26$^{o}$.

The loss coefficient at -4$^{o}$ in subsonic flow is approximately 50% of the loss coefficient at 26$^{o}$. In supersonic flow, the loss coefficients at all incidences have similar magnitudes. At all incident angles, the loss coefficient increased by five times when the exit Mach number is varied from 0.6 to 1.1. However, the incidence losses differed by only 100% at all exit Mach numbers. The effect of flow incidence on losses is secondary compared to the effect of Mach number.

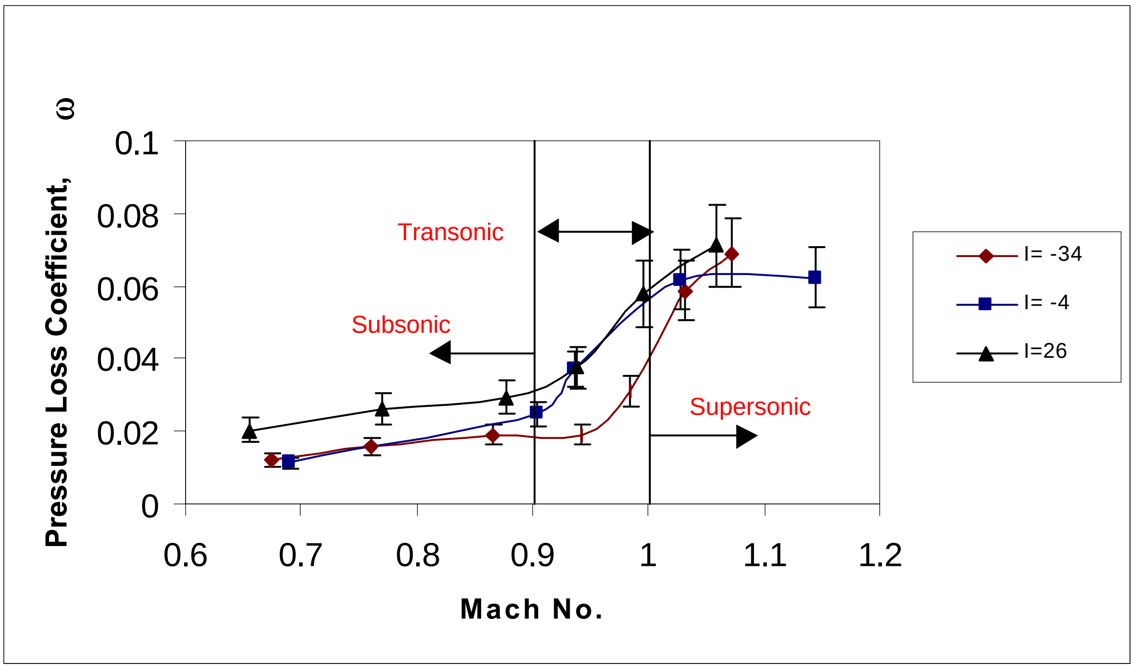


**Figure 4.7 Pressure Loss Coefficient Variation with Exit Mach Number and Incidence, Blade 526A**

## 4.2 Total Pressure Loss Measurements, Blade 525B

This section presents the total pressure measurements and loss results for tested nozzle 525B. The blade geometry of this nozzle is similar to nozzle 526A with the exception of a having a longer nose and the solidity of the cascade is larger than 526A.

### 4.2.1 Downstream Total Pressure Profiles

Figures 4.8 through 4.10 displayed the pressure ratio plots for incident angles $5^o$, $35^o$, $-25^o$ with variation in exit Mach numbers. The design incidence for nozzle 525B is zero degrees. Due to the facility limitation, current setup allows the cascade to be angled at $5^o$ incidence. In this report, this angle will be referred to as near design condition. Pressure data are collected for tunnel runs with exit Mach number varying from 0.61 to 1.12. Generally, the wake trends measured at all exit Mach number demonstrated good periodic flow in the blade passages measured as evidenced by shadowgraphs in Figure 4.11-4.13. The periodicity of the flow for this nozzle is better than nozzle 526A at all incident angles. The high blade solidity for the 525B nozzle allows better flow guidance hence having more periodic exit flow.

At $5^o$ incidence, significant stagnation pressure loss in the freestream between two blades is not pronounced until exit Mach 0.96. At this exit Mach number, the freestream encountered a 2% drop in pressure ratio. Losses in the stagnation pressure ratio in the freestream is 4% at exit Mach 1.12, however, at exit Mach 1.02 this loss is 6%. It is likely that the trailing edge shocks has changed from normal to oblique from exit Mach 1.02 to 1.12. Shadowgraphs shown in Figure 4.11 are taken from exit Mach 0.96 to 1.13. They displayed clearly the progression of shock formation with increasing exit Mach number.

When the cascade is rotated to a $35^o$ incidence, the pressure ratio plots in Figure 4.9 show evident losses in the freestream at exit Mach 0.81. This increased in losses is suspected to be the result of flow separation at the leading edge of the blade. Shadowgraphs taken from exit Mach 0.99 to 1.10 shown in Figure 4.12 show presence of this separation. Freestream stagnation pressure loss is 7% at exit Mach 1.10 and that is 3% higher than the stagnation pressure loss at $5^o$ incidence with similar exit Mach number. This suggests that the losses in the blade passage at $35^o$ incidence due to a combination of shock losses and leading edge separation are considerably higher than at near design angle of $5^o$.

Total pressure data for incident angle of $-25^o$ are presented in Figure 4.10. Starting from exit Mach 0.64, there is evidence supporting stagnation pressure loss in the freestream. Figure 4.13 contains a schlieren picture taken at exit Mach 1.12. This picture does show flow separation from the leading edge of the pressure surface. The point of flow reattachment is not clear from the picture. Freestream stagnation pressure loss at exit Mach 1.12 is 1% lower than exit Mach 1.06. This demonstrated that the shock structure is transforming from normal to oblique.

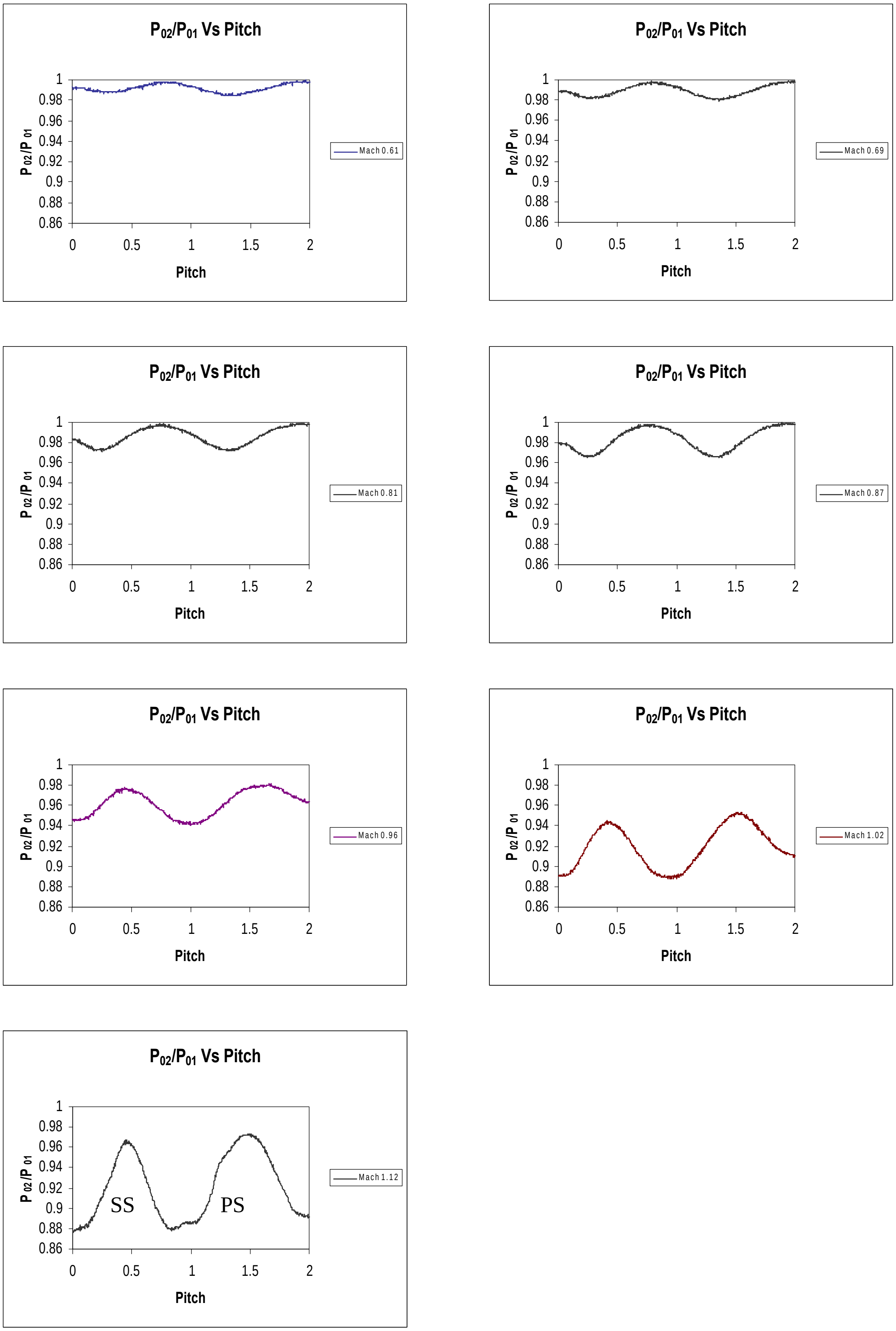


**Figure 4.8 Pressure Ratio at 5° Incidence**

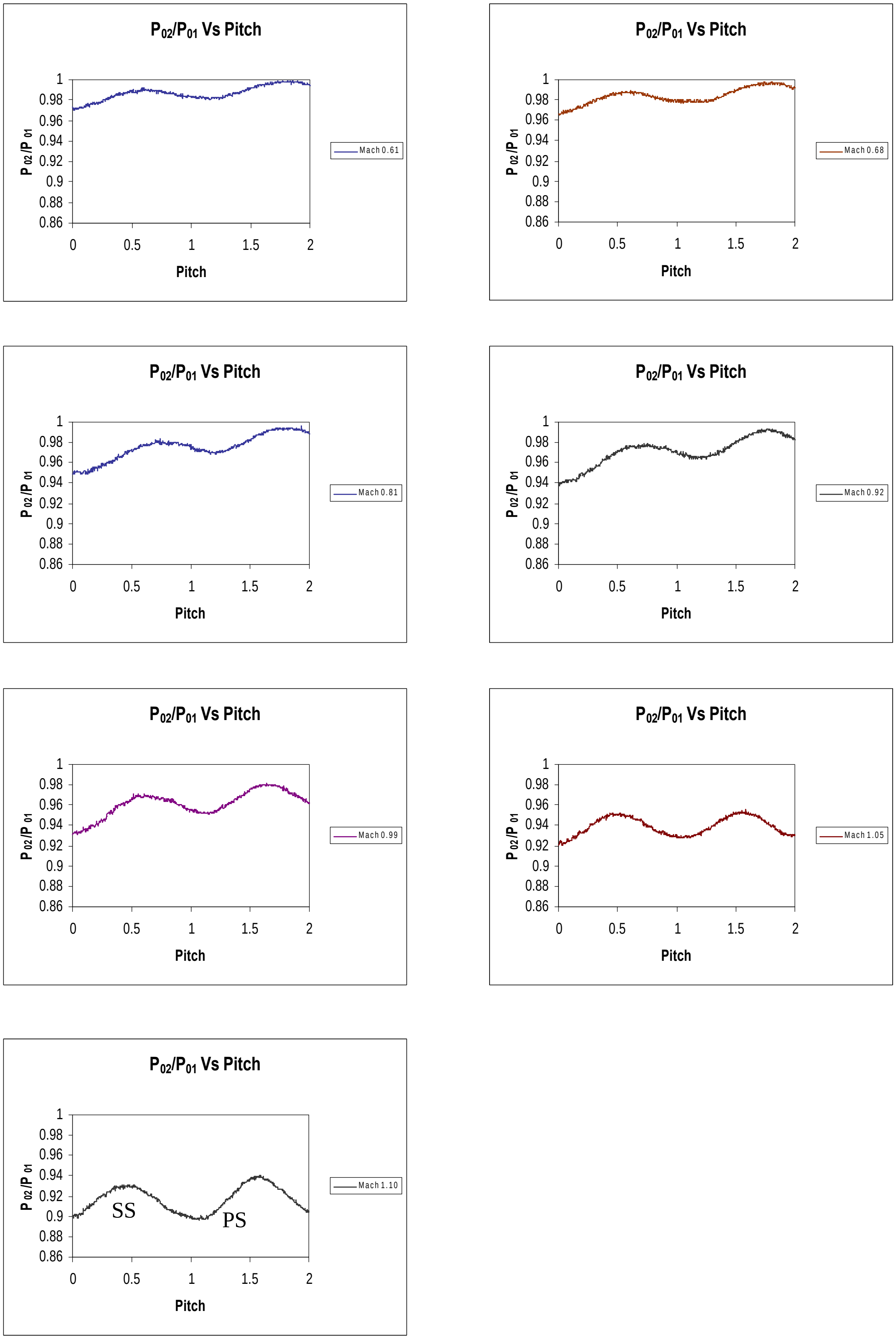


**Figure 4.9 Pressure Ratio at 35$^{o}$ Incidence**

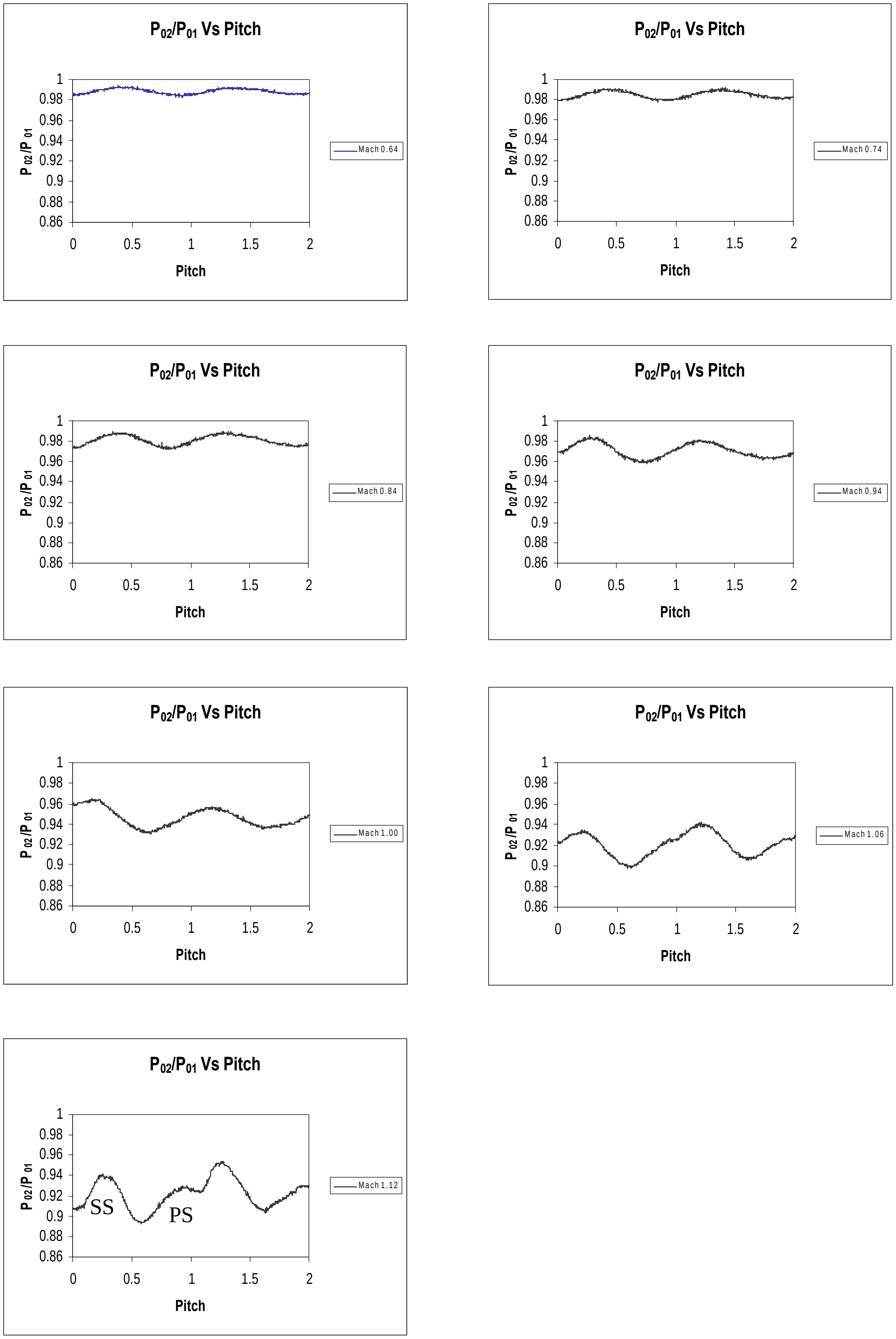


**Figure 4.10 Pressure Ratio at -25° Incidence**

Flow

Direction

No Flow (Reference)

Mach 0.96

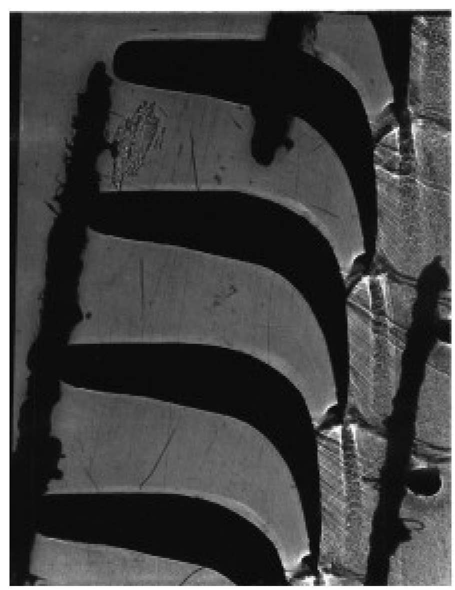

Mach 1.02

Mach 1.12

**Figure 4.11 Shadowgraphs at 5° Incidence**

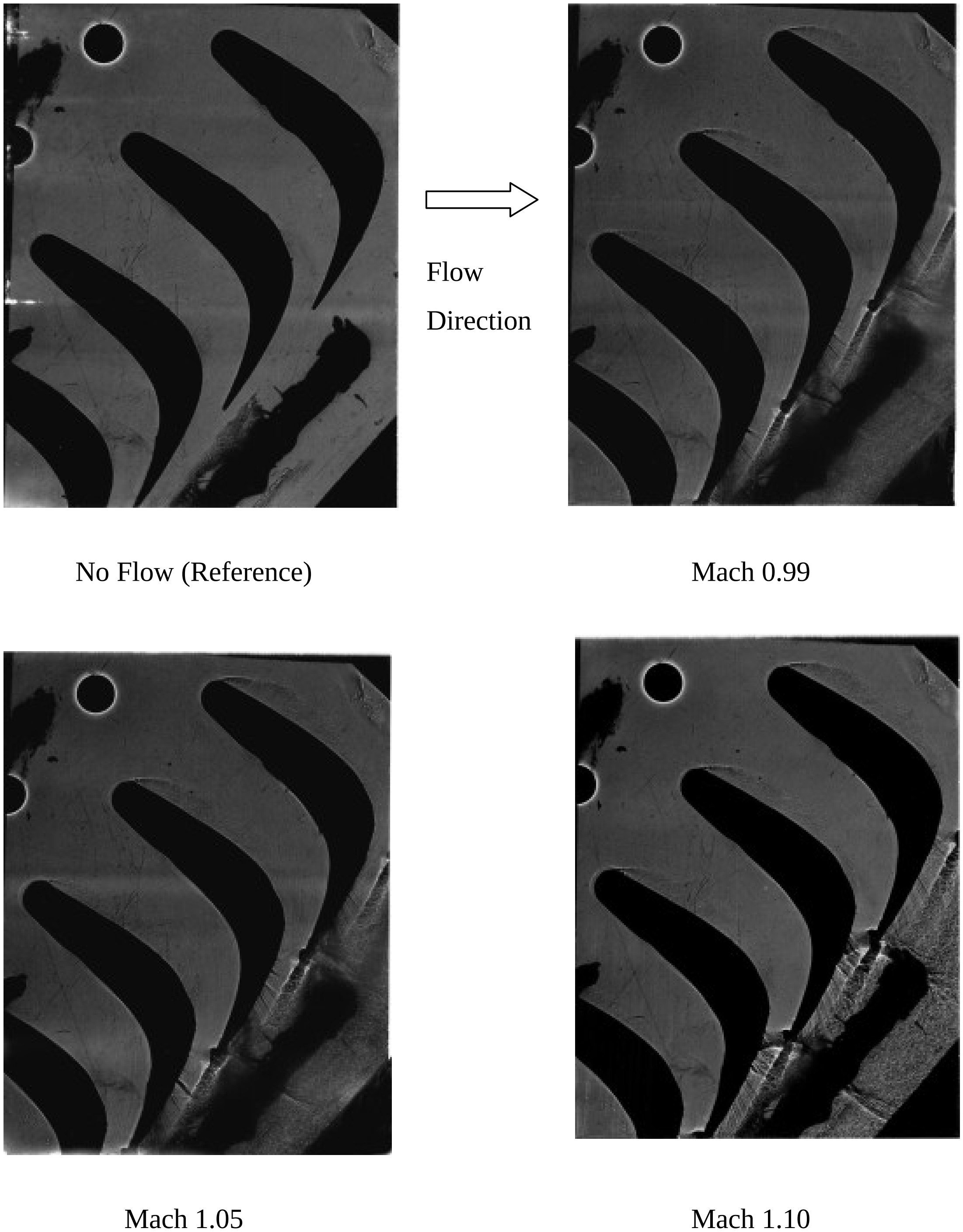


**Figure 4.12 Shadowgraphs at 35° Incidence**

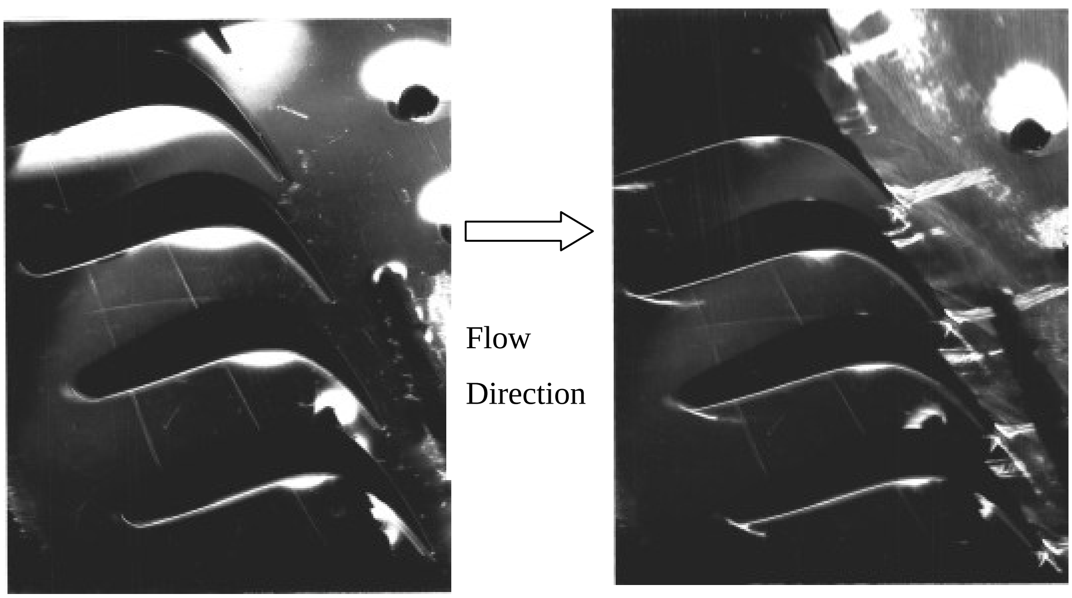


No Flow (Reference) Mach 1.12

**Figure 4.13 Schlierens at -25$^{o}$ incidence**

### 4.2.2 Variation of Profile Loss with Mach Number and Incidence

Figure 4.14 displays the variation in loss coefficient with exit Mach number. Regardless of the extremities in flow incidence, the loss coefficient trend is similar at all three incident angles tested. The largest incident angle tested for this nozzle is $35^o$, whereas for nozzle 526A it is $-34^o$. From exit Mach number ranging from 0.6 to 0.92, the loss coefficient doubled and the trend is rather linear at all the three incident angles. Within this exit Mach number range, $5^o$ incidence demonstrated to have the lowest loss and the $35^o$ incidence having the highest loss, as expected. The loss coefficient at near design is approximately 50% of the losses at off-design in subsonic flow. However, once the exit Mach number exceeds 0.90, the loss pattern is reversed, with $5^o$ incidence having the highest loss and $35^o$ incidence having the lowest loss among the three incident angles. When the exit Mach number reaches 1.1; exit flow is supersonic, the losses at all incident angles have similar magnitudes.

At $5^o$ incidence, the steep increase in loss coefficient occurred between exit Mach 0.87 to 0.96. From Figure 4.11, a shadowgraph taken at exit Mach 0.96 showed the distinctive presence of normal shocks forming on the suction surface of the trailing edge. This figure also displayed flow separation near the trailing edge resulting from the formation of normal shocks. This leads to a thicker wake being shed from the blade, as evidenced in Figure 4.11. These loss generating mechanisms are mainly responsible for the steep increase in the loss coefficient. Shock progression continues to occur when the exit Mach number is increased beyond unity. The loss coefficient peaked at 8.3% at exit Mach 1.02. Subsequently, the loss coefficient at exit Mach 1.12 is 8.1%. Figure 4.11 demonstrates the progression of shock angle from $90^o$ to $70^o$ when the exit Mach number is increased from 0.96 to 1.12. The fishtailed shocks are actually weak oblique shocks and their strength diminishes with decreasing shock angle.

Losses at $-25^o$ incidence are predominantly 50% greater than $5^o$ incidence from exit Mach 0.6 to 0.87. Flow entering the blade passages at this extreme negative incidence will result in flow separation at the pressure surface. A schlieren picture shown in Figure 4.13 displayed flow separation starting from the leading edge and the reattachment point is not clear from the picture. It is likely that the flow will reattach at some point of the pressure surface because of stronger flow acceleration occurring towards the trailing edge. Even though this picture is taken at exit Mach 1.12, it can be assumed that flow separation will also occur at subsonic Mach numbers resulting in higher losses compared to $5^o$ incidence. Beyond exit Mach 0.92, the loss coefficient dips below the loss coefficient at $5^o$ incidence. The loss coefficient eventually peaked at 7.8% at exit Mach 1.06, which is slightly lower than the maximum loss coefficient observed at $5^o$ incidence. It is hypothesized that the shock and shock-boundary layer loss is lower due to presence of less defined trailing edge shocks at exit Mach 1.12. In addition, the flow entering at $-25^o$ incidence demonstrates lower channel acceleration than at $5^o$ incidence. The Mach number ratio, $M_1/M_2$ is higher at this negative incidence.

Suction surface flow separation is a common sign when flow enters the blade passages at extreme positive incidence. The shadowgraphs in Figure 4.12 clearly show flow separation starting from the leading edge on the suction surface. This phenomenon is substantiated by the higher loss coefficient experienced at this angle when compared to $5^o$ incidence in the exit Mach number range of 0.6 to 0.94. At subsequent exit Mach numbers, the loss coefficient dips below the loss coefficients at $-25^o$ and $5^o$ incidence. It is suggested that the leading edge flow separation is strong enough to impede flow acceleration in the blade passages. The $M_1/M_2$ ratio at this incidence also suggested that there is less flow acceleration present compared to the other tested angles. Hence, the shock structure developed at higher Mach exit numbers compared to the other angles. Since shock and shock/boundary layer interaction losses are the governing factors causing steep losses in transonic flow, it is hypothesized that the late shock development at $35^o$ incidence is the main cause for it's loss coefficient to be the lowest when the exit Mach number is around unity. As the inlet Mach number increases, stronger shock structure is quite evident at exit Mach 1.1, as shown by Figure 4.12. At this exit Mach number, the loss coefficient is similar to those at other incident angles.

The impact of flow incidence is again considered secondary to the effects of Mach number. The losses increased by 700% from subsonic to supersonic flow. Losses arising from flow incidence differed by only 100%. Like nozzle 526A, the effects of Mach number are more dominant than flow incidence. Losses for nozzle 526A and 525B appear to display similar trends and magnitudes. Apparently, the similarity in blade geometry might be a factor. This observation will be discussed in further details in the following section.

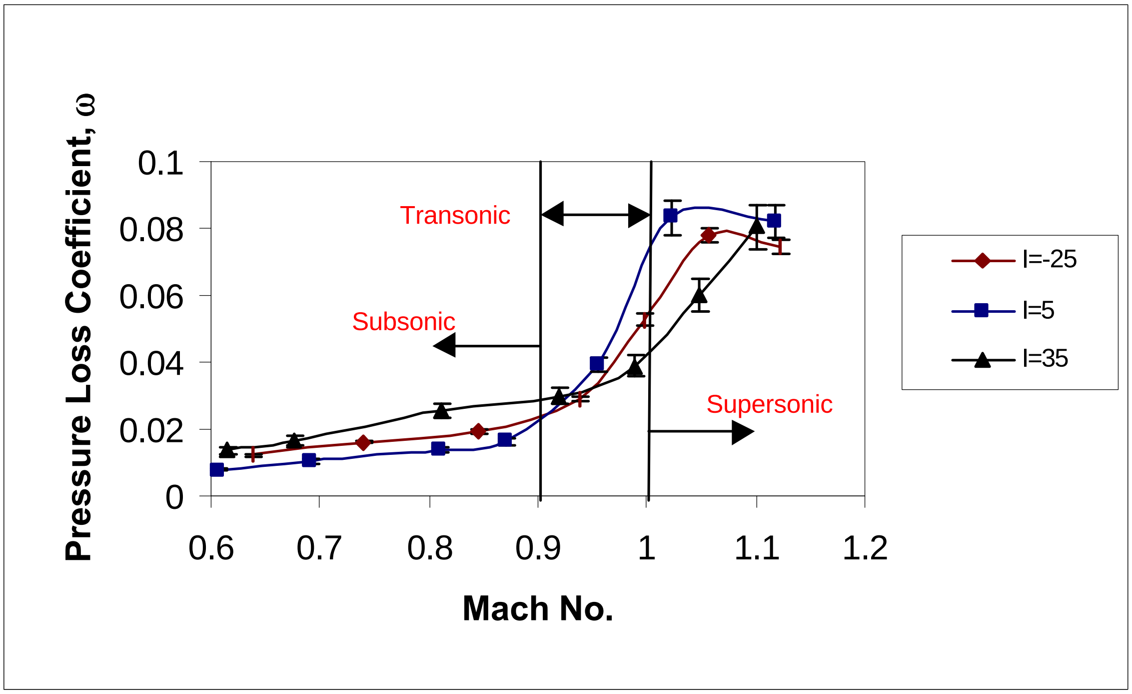


**Figure 4.14 Pressure Loss Coefficient Variation with Exit Mach Number and Incidence, Blade 525B**

## 4.3 Comparison of Current Results with Data in Literature

Turbine cascade tests are performed repeatedly over the years to estimate the performance of turbine blades. The cascade tests performed by researchers can produce results that differ from one another due to the setup of the test facilities. Moreover, it is difficult to obtain test data for blade profiles that matches the profile that the current experiment uses. Blade profiles of different family and design can produce different variation in profile losses. Data currently available for comparison to the current nozzles tested at VPI are obtained from Von Karman Institute(VKI) (Kiock, 1985) and from Indian Institute of Technology(IIT) (Venkatrayulu, 1989). These turbine blades are used in fifty percent reaction stages and are designed to operate at an exit Mach number of approximately 0.8. The blade geometry is rather similar to the current nozzles tested. Figure 4.15 display blade profile for nozzles 526A, 525B and turbine blades from VKI and IIT. The inlet metal angle is $74^o$ and the exit metal angle is $20^o$ for blade from IIT whereas the blade from VKI has inlet metal angle of $60^o$ and exit metal angle of $23^o$. The loss data presented by VKI and IIT are in terms of energy loss coefficients. They are changed to the total pressure loss correlation used in this investigation for comparison. It is apparent that the loss coefficients from the various turbine blades in Figure 4.16 agree well with one another. The loss trend from the different profiles demonstrated similar pattern when varied with exit Mach number. The losses looked quite constant at subsonic Mach numbers but increased steeply at near sonic exit Mach numbers. Even though the turbine blades from VKI and IIT are designed for exit Mach 0.8, losses are lower at exit Mach numbers below 0.8 according to the pressure loss coefficient used to the interpret the data. Among the four blade profiles, the profile from IIT has the lowest losses at exit Mach number below 0.85. The leading edge curvature of the blade from IIT is smoother and has a larger radius. The passage between blades is not as convergent as nozzle 526A and 525B. Hence, suggesting that flow acceleration within blade passages is not as pronounced as the other blade profiles. It is hypothesized that the boundary layer is predominantly laminar for most part of the suction surface with transition occurring towards the trailing edge. Thus, losses for this blade profile are lower than the rest. The loss data from VKI falls exactly on the loss obtained for nozzle 526A from exit

Mach number ranging from 0.57 to 0.95. This might be due to the similarity in blade design shared by the two profiles.

Nozzle 526A and 525B belongs to a similar blade family. Although their blade shapes looked quite different, their inlet and exit blade angles are nearly the same. In addition, the throat/pitch ratio is identical, suggesting similar flow accelerating conditions in the blade passages. At closer look at Figure 4.16(a) shows that the losses at subsonic exit Mach number is a little lower for nozzle 525B, but when the exit Mach number exceeds unity the trend reverses with nozzle 525B experiencing much higher losses. The rear suction side curvature is a major factor in determining losses in convergent cascade. Researchers such as Ainley and Mathieson have concluded that larger curvature at the blade tail section exhibits high losses at supersonic exit Mach numbers due to the shock induced separation of the laminar boundary layer. Blades of larger trailing edge curvature tend to over accelerate resulting in flow separation. At subsonic exit flow, blades with trailing edge curvature will experience a laminar boundary layer as the peak suction side velocity will be moved towards the trailing edge. Hence, straight-backed blades will generally exhibit higher losses at low Mach numbers because of the position of the maximum velocity on the suction surface. The trailing edge curvature for nozzle 525B is greater than that of 526A and the loss coefficient trend is similar to those mentioned by Ainley and Mathieson. The loss coefficient for nozzle 525B is lower than 526A from exit Mach 0.7 to 0.98. Subsequently, the losses for nozzle 525B supercede 526A by 30% when the exit Mach number exceeds beyond unity. From the shadowgraphs shown in Figure 4.11, the presence of pressure surface shocks impinging onto the suction surface is more evident for nozzle 525B. Localized boundary layer separation is expected on the impinged surface with the boundary layer turning turbulent after the reflected shocks. These are physical evidence representing the large difference in losses between nozzle 525B and 526A at supersonic exit Mach numbers. For this current investigation, the losses associated with shock-boundary layer interaction are believed to be the main component leading to increased profile loss at supersonic exit Mach numbers.

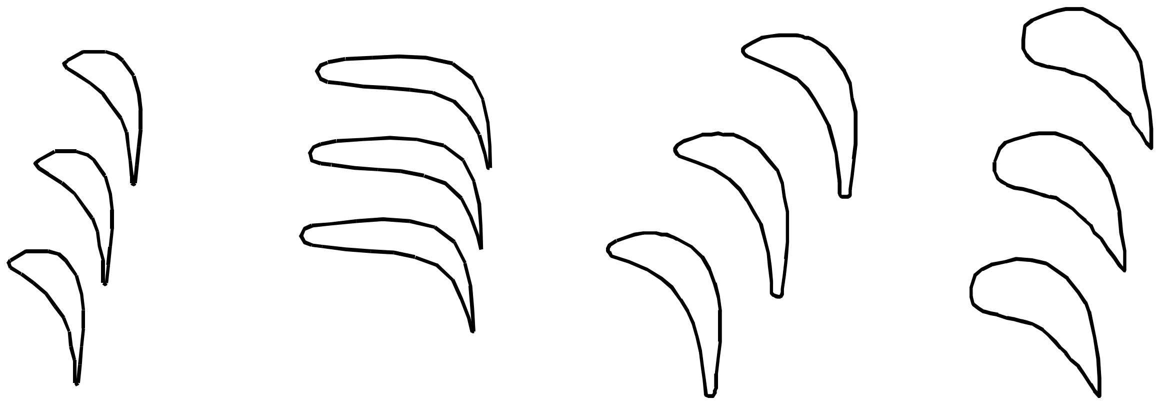

526A 525B (VKI, 1985) (IIT, 1989)

**Figure 4.15 Blade Profiles**

**Table 4.1 Blade Specifications from Literature**

| **Type** | 526A | 525B | VKI | IIT |
|---|---|---|---|---|
| **$\beta_1$** | $76.4^o$ | $85^o$ | $60^o$ | $74^o$ |
| **$\alpha_2$** | $11.54^o$ | $12^o$ | $23^o$ | $20^o$ |
| **solidity** | 1.34 | 2.15 | 1.41 | 1.17 |
| **gauging** | 0.2 | 0.2 | 0.38 | N/A |

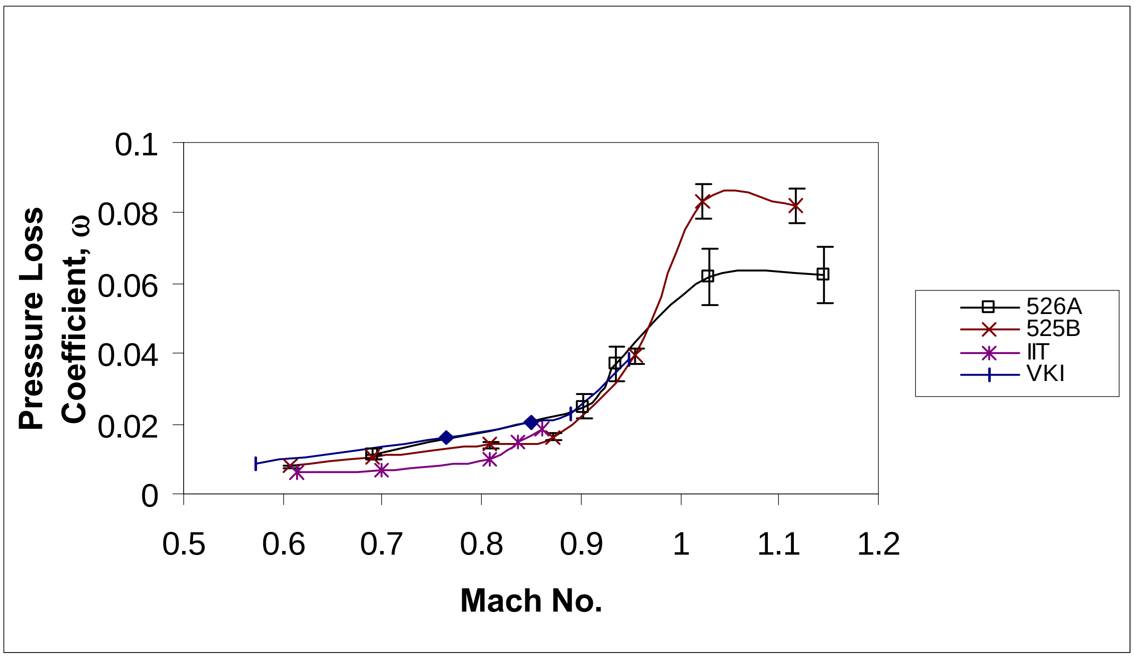


**Figure 4.16(a) Comparison with Existing Data at Near Design Incidence**

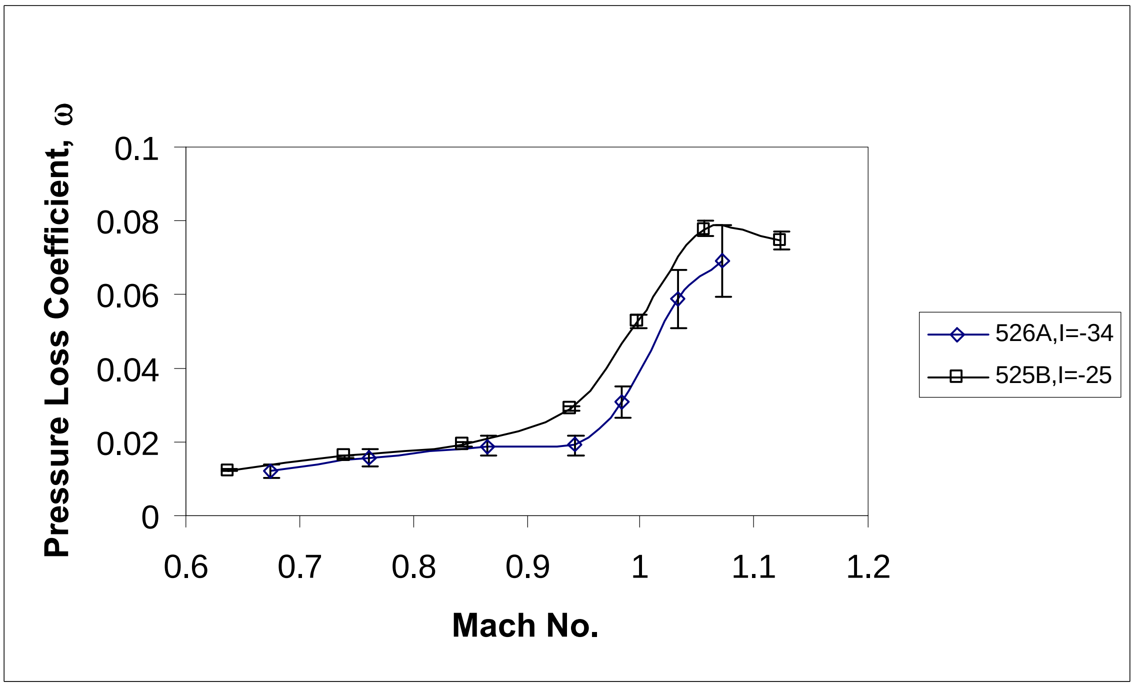


**Figure 4.16(b) Comparison with Existing Data at Extreme Negative Incidence**

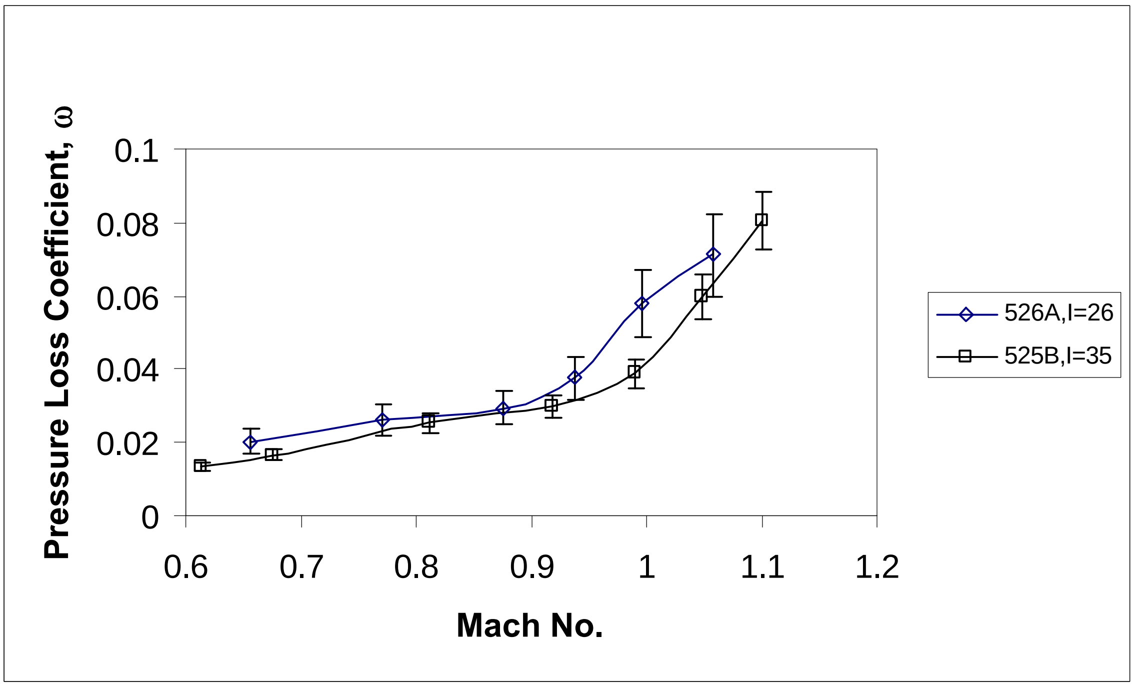


**Figure 4.16(c) Comparison with Existing Data at Extreme Positive Incidence**

The loss coefficient for nozzle 525B at -25$^{o}$ and that for nozzle 526A at -34$^{o}$ are shown in Figure 4.16(b). Losses at these extreme negative incidences are quite similar till exit Mach 0.85. Losses for nozzle 525B exceed that of nozzle 526A by 15% beyond exit Mach 0.85. It seems that nozzle 526A is more effective operating at negative incidence than nozzle 525B. Stronger shock boundary layer losses incurred by nozzle 525B due to its larger trailing edge curvature is suggested as the main reason for the high losses.

The loss coefficients for nozzle 525B at 35o and for nozzle 526A at 26o are presented in Figure 4.16(c). At positive incidence the loss coefficient for nozzle 525B at 35$^{o}$ is lower than that for nozzle 526A at 26$^{o}$ at all exit Mach numbers. An explanation for this occurrence is not known at this point.

## 4.4 Comparison with Prediction Method

The loss correlation formulated by Kacker and Okapuu(1981) is used to calculate the profile losses for nozzle 526A and 525B. This method refines Ainley-Mathieson(1951) correlation to account for Mach number effects, channel acceleration and also for the advances in turbine design over the past three decades. The Ainley-Mathieson method correlates profile loss as a function of exit flow angle and blade solidity. The profile loss at zero incidence is as follows,

$$\omega_{p,amdc} = \left( Y_p(\beta_1 = 0) + \left|\frac{\beta_1}{\alpha_2}\right| \left(\frac{\beta_1}{\alpha_2}\right) \left[ Y_p(\beta_1 = \alpha_2) - Y_p(\beta_1 = 0) \right] \right) \left( \frac{t_{max}/c}{0.2} \right)^{\beta_1/\alpha_2} \qquad (4.1)$$

The loss coefficient for nozzles or impulse blades can be obtained from [1]. Losses for turbine blades of different degree of reaction can be calculated from equation 4.1. The first term in equation 4.1 account for the profile loss at design condition while the second term depend on the blade shape and turning. The multiplier is a correction factor for blade thickness to chord ratio. In determining the profile loss for nozzles, the first term is the dominating factor. For losses at off-design conditions, they are dependent on the stalling incidence of the nozzle. Stalling incidence is a condition where the profile loss at this instance is twice the magnitude of the profile loss at design condition. The figure correlating profile loss at off-design condition with stalling incidence is found in [1].

The Kacker-Okapuu loss prediction method developed some thirty years after the released of the Ainley-Mathieson loss correlation is given below.

$$\omega_{p,ko} = 0.914\left(\frac{2}{3}\omega_{p,amdc}\left(1-\left[\frac{M_1}{M_2}\right]^2(1.25(M_2-0.2))\right)\right)\times\omega_{shock} \tag{4.2}$$

$$\omega_{shock} = 1 + 60(M_2 - 1)^2 \tag{4.3}$$

The 2/3 multiplier is a correction factor for recent improvement in blade design. Within the larger parenthesis with variables such as inlet and exit Mach numbers is the loss factor due to channel acceleration. Equation 4.3 is the loss correlation for supersonic drag rise when the exit Mach number exceeds unity. An improvement on the shock loss relation from Kacker and Okapuu is developed from current experimental data. The shock loss is assumed to vary linearly with the exit Mach number. The correlation below is valid when the the exit Mach number is greater than 0.94.

$$\omega_{shock} = 15.3M_2 - 12.5 \tag{4.4}$$

Figures 4.17 and 4.18 display the losses calculated by Kacker and Okapuu correlation with the experimental losses and the proposed revision for the shock model used by Kacker and Okapuu. At all incident angles for both nozzles, the Kacker-Okapuu prediction method has underestimated the losses, especially at supersonic exit Mach numbers. Among the two nozzles, the prediction method is able to estimate the losses at near design and extreme negative incidence satisfactorily at Mach numbers below unity. At exit Mach number beyond unity the Kacker-Okapuu shock model severely underestimated the loss, whereas the proposed shock model is accurate within ±30%. In extreme positive flow incidence, the Kacker-Okapuu(KO) method is inadequate at all exit Mach numbers. However, the proposed shock model matched better with the experimental losses at exit Mach number greater than 0.9.

The inability of the KO method to predict losses at positive incidence might be due to the following. The prediction method employed by Kacker and Okapuu is designed to predict losses at zero incidence first before the losses at off-design incidences can be calculated based on stalling incidence of the blade profile. The graph used to correlate losses at off-design incidences with stalling incidence is derived from turbine blades designed several decades ago. This figure has to be revised to account for advancement in turbine blade design to better estimate profile losses of current turbine blades. At supersonic exit Mach numbers, a simple parabolic relation in terms of exit Mach number such as equation 4.3, is used to predict losses due to formation of shocks and shock boundary layer interaction. As evidence from Figures 4.17 and 4.18, this form of shock loss prediction clearly underestimated the losses compared to the experimental data. The key components that account for losses at supersonic exit Mach numbers are flow separation and shock boundary layer interaction. These structures are too complicated to be analyzed using simple shock relations. The current proposed shock model, although purely empirical based, managed to account for the losses in transonic flow more accurately. This should not come as a surprise since the current proposed shock model is simply a curve fit to provide the best match to the data for all incident angles and exit Mach numbers. It should be aware that this proposed shock model is validated for the current set of tested nozzles only.

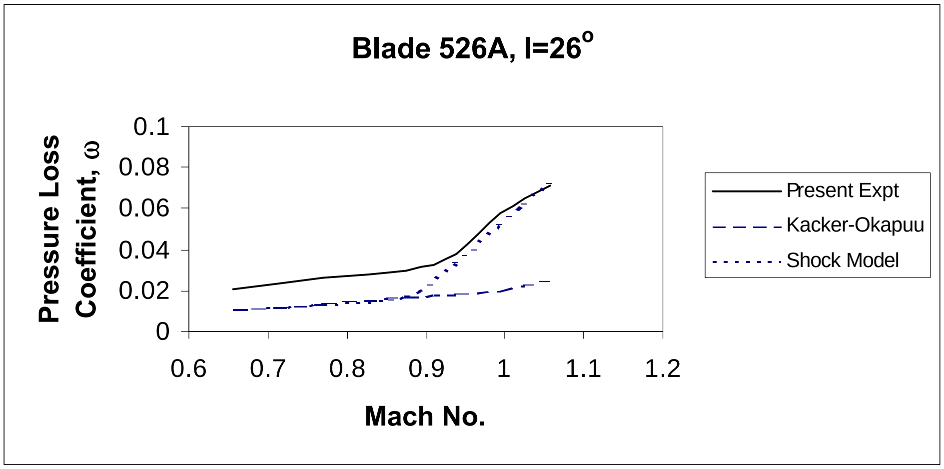


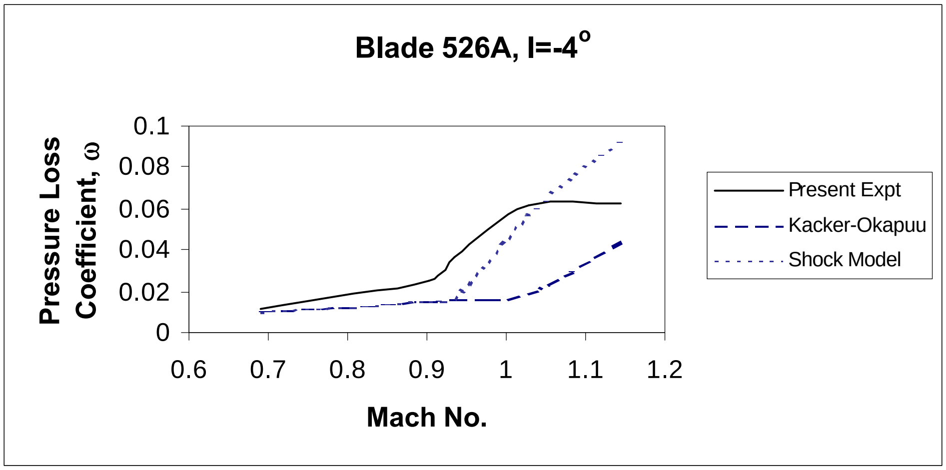


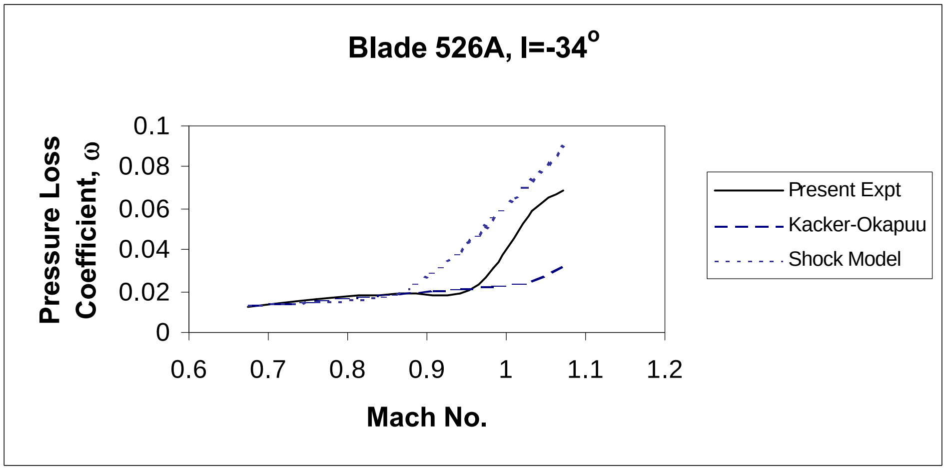


**Figure 4.17 Comparison with Prediction Method for 526A**

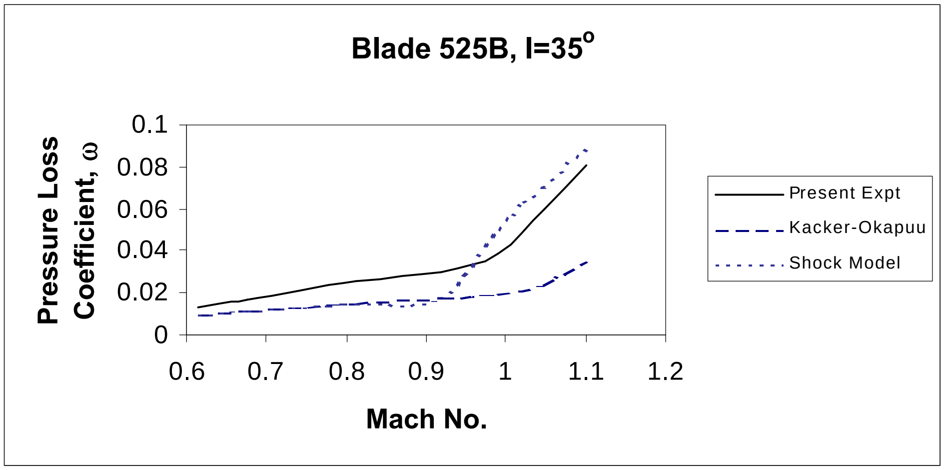


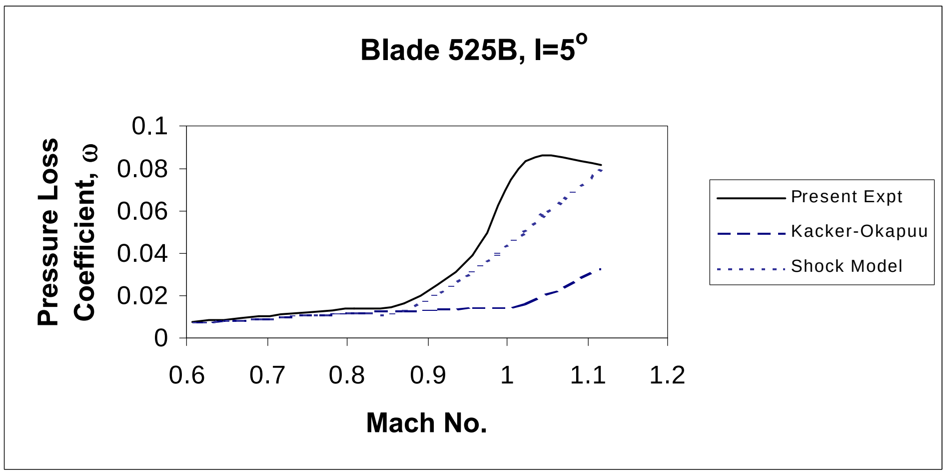


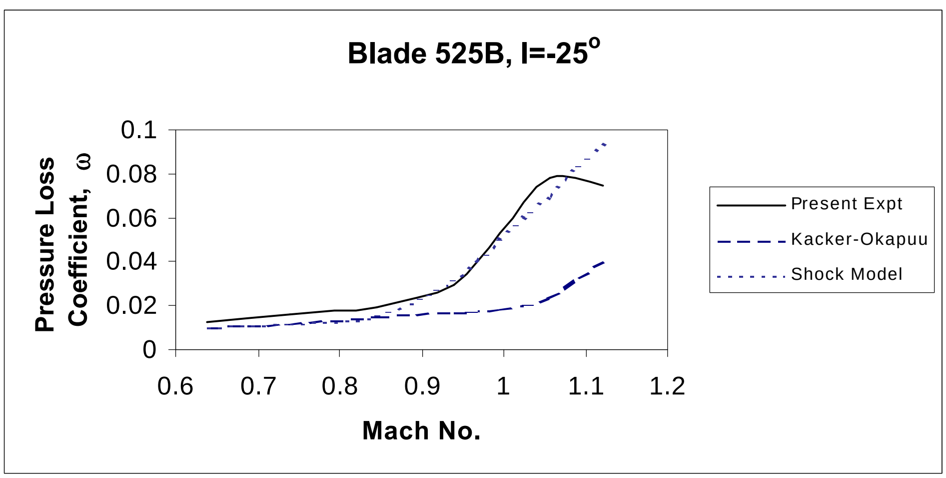


**Figure 4.18 Comparison with Prediction Method for 525B**

# Chapter 5 CONCLUSION

The influence of extreme flow incidence and Mach number on profile losses is investigated for two steam turbine nozzles.  The inlet flow incidences are varied from $-34^{o}$ to $35^{o}$ for the two cascades and the exit Mach number ranged from 0.6 to 1.15. Trends for profile loss variation with exit Mach numbers are similar at all tested angles for both nozzles.  Losses are rather constant at subsonic Mach numbers due to accelerating flow and a thin boundary layer from a favorable pressure gradient.  In transonic flow the profile losses increased steeply due to the formation of trailing edge shocks and shock induced boundary layer separation.  When the exit flow goes supersonic, the losses peaked and decreased subsequently due to the transformation of the stronger normal shock into weaker oblique shocks.  However, there are instances at positive incidence where the losses continued to rise.

For both nozzles tested at subsonic Mach numbers, the profile loss at near design incidence is always the lowest.  Losses at extreme positive incidence are always the highest and the periodicity in the flow is the worst among the other angles.  However, at higher Mach numbers in transonic flow, the losses at off-design incidence is lower than design.  This trend is attributed to the later formation of shocks and subsequent boundary layer separation at high Mach numbers.  Channel acceleration is most favorable at design incidence, as evidence by their low $M_1/M_2$ ratio.  Moreover, the nozzles tested are curved backs and they encourage over-acceleration at the trailing edge, which result in shock formation and boundary layer separation occurring at Mach numbers below unity.   When the exit flow goes supersonic in the Mach number range of 1.05 to 1.10, the losses at all incident angles have similar magnitudes.  Shadowgraphs show that at those exit Mach numbers, the shock structure at all angles looked more developed and somewhat similar. This observation is noted for both nozzles tested.

In the Mach number range of 0.6 to 1.15, the losses increased by 600%-700% for the steam turbine nozzles tested.  However, the losses due to incidence only differed by 100%.  Clearly, the effects of Mach number are more predominant than flow incidence when the nozzles are operated under transonic or supersonic conditions. Shock/boundary layer interaction is believed to be the key component in escalating the losses under the above conditions.

The validity of the test data obtained from VPI's transonic cascade is reaffirmed by test data obtained from VKI and IIT. The turbine blades from VKI and IIT have similar geometry and their profile losses are quite similar with losses from nozzle 526A and 525B at subsonic exit Mach numbers. Even though nozzle 526A and 525B have quite different blade shapes, their profile losses at sub-unity exit Mach numbers are nearly identical. At supersonic exit Mach numbers, the profile losses for 525B are much higher due to its larger trailing edge curvature which causes over acceleration. This also causes a larger pressure difference to exist between the suction and pressure surfaces at the trailing edge resulting in flow separation induced by formation of shocks. Shadowgraph studies presented evidence supporting that stronger shocks are formed at the trailing edge for nozzle 525B, hence the higher losses in supersonic exit flow.

The prediction method from Kacker and Okapuu has adequately predicted the profile losses for the two nozzles in subsonic conditions for near design and negative incidence. However, the shock model by Kacker and Okapuu is ineffective in estimating losses at higher Mach numbers. This method severely underpredicted losses at $M_2>0.9$ by 300%. At extreme positive incidence the model is inadequate in predicting losses at all Mach numbers. The proposed shock model devised from current experimental data is accurate within ±30% of experimental data.

Possible future direction in this work will be to investigate the effect of aspect ratio on the aerodynamic losses of the steam turbine nozzles. The nozzles tested at VPI are much longer than those used in the actual steam turbine. When the aspect ratio is decreased, secondary losses arising from 3-D flow field within the blade passages can affect the overall loss.

## REFERENCES


1. Ainley, D. G., and Mathieson, G. C. R., 1951, “A Method of Performance Estimation for Axial Flow Turbines”, British ARC, R&M 2974

2. Ainley, D. G., 1948, “The Performance of Axial Flow Turbines”, Proceedings of the Institution of Mechanical Engineers, Vol. 159

3. Chen, S., 1987, “A Loss Model for the Transonic Flow Low-Pressure Steam Turbine Blades”, Institute of Mech. Engrs. C269

4. Craig, H. R. M., and Cox, H. J. A., 1971, “Performance Estimate of Axial Flow Turbines”, Proceedings of the Institution of Mechanical Engineers, Vol. 185, No. 32, pp. 407-424

5. Goobie, S., Moustapha, S. H., and Sjolander, S. A., 1989, “An Experimental Investigation of the Effect of Incidence on the Two-Dimensional Performance of an Axial Turbine Cascade”, ISABE Paper No. 89-7019

6. Hodson, H. P., and Dominy, R. G., 1986, “The Off-Design Performance of a Low Pressure Steam Turbine Cascade”, ASME Paper No. 86-GT-188

7. Kacker, S. C., and Okapuu, U., 1981, “A Mean Line Prediction Method for Axial Flow Turbine Efficiency”, ASME Paper No. 81-GT-58

8. Kiock, R., Lehthaus, F., Baines, N. C., Sieverding, C. H., 1985, “The Transonic Flow Through a Plane Turbine Cascade as Measured in Four European Wind Tunnels”, ASME Paper No. 85-IGT-44

9. Lakshminarayana, B. Fluid Dynamics and Heat Transfer of Turbomachinery. New York: John Wiley & Sons, 1996.

10. Mee, D. J., Baines, N. C., Oldfield, M. L. G., and Dickens, T. E., 1990, “An Examination of the Contributions to Loss on a Transonic Blade Cascade”, ASME Paper No. 90-GT-264

11. Venkatrayulu, N., Dasgupta, A., and Srivastava, K. M., 1989, “Studies on the Influence of Mach number on Profile Losses of a Reaction Turbine Cascade”, ISABE Paper No. 89-7016

# APPENDIX

## Uncertainty Analysis

The experimental uncertainties for the cascade test consist of two categories. The first being the uncertainty arising from the accuracy of data acquisition equipment such as pressure transducers and thermocouples. Secondly, due to aperiodicty of the exit flow, the averaged loss coefficient of two blade passage has uncertainty too.

The first source of error from uncertainty of instruments is reflected on the measured and calculated parameters such as total pressure, differential pressure, static pressure Mach numbers, and loss coefficient. The uncertainties due to instrument error are:

$\delta P_{o1} = \pm 0.036$ psi

$\delta Ps = \pm 0.03$ psi

$\delta Pd = \pm 0.01$ psi

$\delta T_{o1} = \pm 1$ K

Uncertainty for the calculated loss coefficient is a function of the following parameter,

$\delta\omega = F(\delta P_{o1}, \delta Pd, \delta Ps, \delta T_{o1})$

Uncertainty for the exit Mach number is a function of,

$\delta M_2 = F(\delta P_{o1}, \delta Pd, \delta Ps)$

The equations use to evaluate the uncertainties are as follow,

$$\delta\omega = \sqrt{\left[\left[\left(\frac{\partial\omega}{\partial P_{o1}}\right)\delta P_{o1}\right]^2 + \left[\left(\frac{\partial\omega}{\partial T_{o1}}\right)\delta T_{o1}\right]^2 + \left[\left(\frac{\partial\omega}{\partial Pd}\right)\delta Pd\right]^2 + \left[\left(\frac{\partial\omega}{\partial Ps}\right)\delta Ps\right]^2\right]}$$

$$\delta M_2 = \sqrt{\left[\left[\left(\frac{\partial M_2}{\partial P_{o1}}\right)\delta P_{o1}\right]^2 + \left[\left(\frac{\partial M_2}{\partial Pd}\right)\delta Pd\right]^2 + \left[\left(\frac{\partial M_2}{\partial Ps}\right)\delta Ps\right]^2\right]}$$

The uncertainties for the loss coefficients and the exit Mach numbers ranging from exit Mach 0.6-1.15 are presented below. These uncertainties are applicable to nozzle 526A and 525B and at all incident angles tested.

The uncertainties for the loss coefficient are

$\delta\omega = \pm 0.360\% - \pm 0.745\%$

The uncertainties for the exit Mach number are

$\delta M_2 = \pm 0.83\% - \pm 0.86\%$

Aperiodicty in the exit flow behind the blade passages contributes to the uncertainty in the averaged loss coefficient and averaged exit Mach numbers of the two blade passage measured. These uncertainties are derived from the absolute difference between the measured quantities from the two blade passages and the averaged value from the two blade passages. The range of uncertainties due to aperodicity at all exit Mach numbers and incident angles are,

$\delta\omega = \pm 2.93\% - \pm 15.64\%$
$\delta M_2 = \pm 0.66\% - \pm 0.99\%$

The uncertainties for the loss coefficient due to aperiodicity are much greater than uncertainties due to the precision error from the measuring instruments. Hence, they are presented as the primary source of error in the loss coefficient calculations. The accuracy of the cascade setup for a particular incident angle is estimated to be within a degree and has negligible effects on the other calculated uncertainties.

## Kinetic Energy Loss Coefficients

The kinetic energy loss coefficient is a common term use to document the losses observed in a turbine cascade. The equation for this method of calculation is mentioned in chapter three. The variation for the kinetic energy loss coefficient with Mach number and flow incidence for nozzle 526a and 525B are presented in Figure A.1 and Figure A.2 respectively.

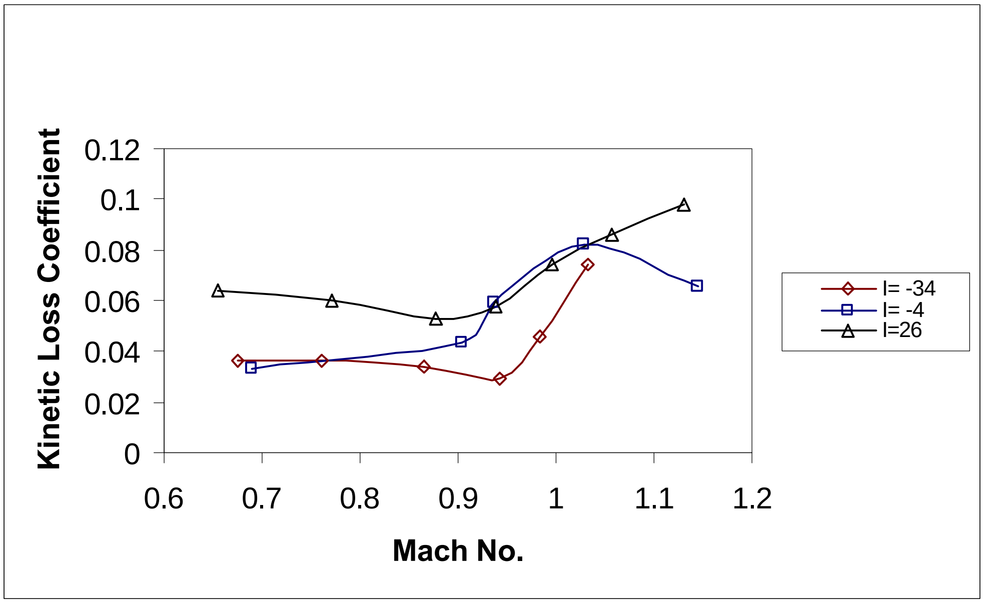


**Figure A.1 Variation of Kinetic Loss Coefficient with Exit Mach number and Incidence, Blade 526A**

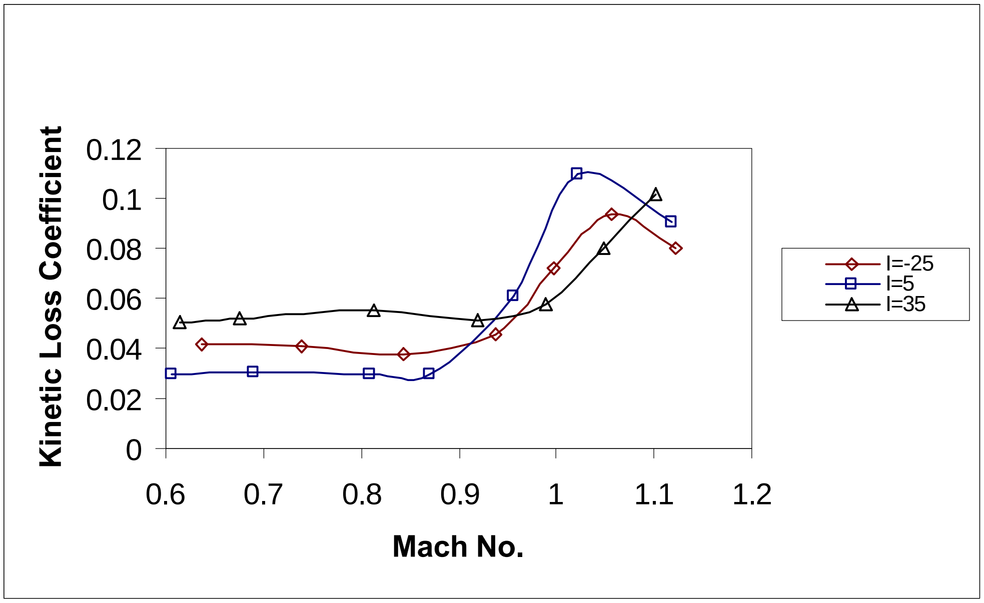


**Figure A.2 Variation of Kinetic Loss Coefficient with Exit Mach number and Incidence, Blade 525B**

The following tables contain the numerical results of the key parameters used in this investigation.

**Table A.1 Numerical Results for Blade 526A, i = - 34**

| Inlet Mach No. | Exit Mach No. | $K.E_{losses}$ | $P_{losses}$ | Re's No. |
|---|---|---|---|---|
| 0.0820 | 0.6753 | 0.0360 | 0.0123 | 755374 |
| 0.1118 | 0.7613 | 0.0367 | 0.0158 | 851686 |
| 0.1363 | 0.8652 | 0.0342 | 0.0190 | 962071 |
| 0.1438 | 0.9422 | 0.0293 | 0.0191 | 1042103 |
| 0.1488 | 0.9845 | 0.0458 | 0.0310 | 1096244 |
| 0.1738 | 1.0327 | 0.0738 | 0.0587 | 1163942 |
| 0.1727 | 1.0718 | 0.0898 | 0.0690 | 1237152 |

**Table A.2 Numerical Results for Blade 526A, i = - 4$^{o}$**

| Inlet Mach No. | Exit Mach No. | $K.E_{losses}$ | $P_{losses}$ | Re's No. |
|---|---|---|---|---|
| 0.0865 | 0.6897 | 0.0331 | 0.0113 | 743915 |
| 0.0915 | 0.9032 | 0.0438 | 0.0248 | 958734 |
| 0.1051 | 0.9358 | 0.0591 | 0.0370 | 989129 |
| 0.1504 | 1.0285 | 0.0824 | 0.0618 | 1071428 |
| 0.2043 | 1.1446 | 0.0659 | 0.0624 | 1316105 |

**Table A.3 Numerical Results for Blade 526A, i = 26$^o$**

| Inlet Mach No. | Exit Mach No. | $K.E_{losses}$ | $P_{losses}$ | Re's No. |
|---|---|---|---|---|
| 0.2097 | 0.6558 | 0.0637 | 0.0204 | 748067 |
| 0.2022 | 0.7709 | 0.0599 | 0.0262 | 886369 |
| 0.1881 | 0.8766 | 0.0526 | 0.0296 | 1010178 |
| 0.2400 | 0.9378 | 0.0579 | 0.0375 | 1083784 |
| 0.2302 | 0.9953 | 0.0745 | 0.0580 | 1149504 |
| 0.2666 | 1.0581 | 0.0861 | 0.0711 | 1223114 |
| 0.2540 | 1.1306 | 0.0975 | 0.0920 | 1320018 |

**Table A.4 Numerical Results for Blade 525B, i = - 25$^o$**

| Inlet Mach No. | Exit Mach No. | $K.E_{losses}$ | $P_{losses}$ | Re's No. |
|---|---|---|---|---|
| 0.1462 | 0.6375 | 0.0414 | 0.0123 | 907818 |
| 0.1783 | 0.7391 | 0.0406 | 0.0161 | 1050110 |
| 0.1960 | 0.8442 | 0.0379 | 0.0195 | 1181911 |
| 0.2116 | 0.9385 | 0.0457 | 0.0291 | 1314432 |
| 0.2137 | 0.9966 | 0.0721 | 0.0527 | 1384547 |
| 0.2151 | 1.0571 | 0.0936 | 0.0778 | 1470157 |
| 0.2184 | 1.1223 | 0.0802 | 0.0745 | 1586576 |

**Table A.5 Numerical Results for Blade 525B, i = 5$^o$**

| Inlet Mach No. | Exit Mach No. | $K.E_{losses}$ | $P_{losses}$ | Re's No. |
|---|---|---|---|---|
| 0.0666 | 0.6065 | 0.0295 | 0.0078 | 871003 |
| 0.0862 | 0.6908 | 0.0304 | 0.0104 | 989584 |
| 0.1103 | 0.8083 | 0.0299 | 0.0140 | 1150235 |
| 0.1407 | 0.8711 | 0.0300 | 0.0163 | 1242819 |
| 0.1694 | 0.9557 | 0.0606 | 0.0393 | 1358956 |
| 0.1598 | 1.0224 | 0.1092 | 0.0831 | 1427312 |
| 0.1510 | 1.1179 | 0.0902 | 0.0820 | 1558373 |

**Table A.6 Numerical Results for Blade 525B, i = 35$^o$**

| Inlet Mach No. | Exit Mach No. | $K.E_{losses}$ | $P_{losses}$ | Re's No. |
|---|---|---|---|---|
| 0.1561 | 0.6142 | 0.0506 | 0.0135 | 874173 |
| 0.1685 | 0.6763 | 0.0517 | 0.0167 | 960148 |
| 0.1783 | 0.8122 | 0.0549 | 0.0253 | 1131872 |
| 0.1913 | 0.9187 | 0.0509 | 0.0299 | 1253870 |
| 0.2023 | 0.9897 | 0.0579 | 0.0389 | 1351013 |
| 0.2099 | 1.0482 | 0.0803 | 0.0598 | 1417981 |
| 0.2242 | 1.1010 | 0.1018 | 0.0805 | 1477271 |

## Vita

Teik Lin Chu was born on December 10th, 1972 in Singapore. Mr. Chu completed his high school at Tampines Junior College in 1990 and subsequently served his national service as a signals specialist for 2 years. From August 1994 until May 1997, Mr. Chu attended college at Christian Brothers University(CBU) and graduated Suma Cum Laude in Mechanical Engineering. He is a active member of the ASME chapter and a collegiate tennis player for 2 years at CBU. In August 1997 he started his graduate studies at Virginia Tech under the guidance of Dr. Wing Fai Ng, specializing in turbomachinery. The author defended his work on March 31st, 1999.